Y. Xie, X. W. Lou et al.

DOI: 10.1002/anie.201303971

Mixed Metal Oxides

Mixed Transition-Metal Oxides: Design, Synthesis, and Energy-Related Applications

Changzhou Yuan, Hao Bin Wu, Yi Xie, and Xiong Wen (David) Lou**

Keywords:
energy storage/conversion · lithium-ion batteries · mixed metal oxides · oxygen reduction · supercapacitors

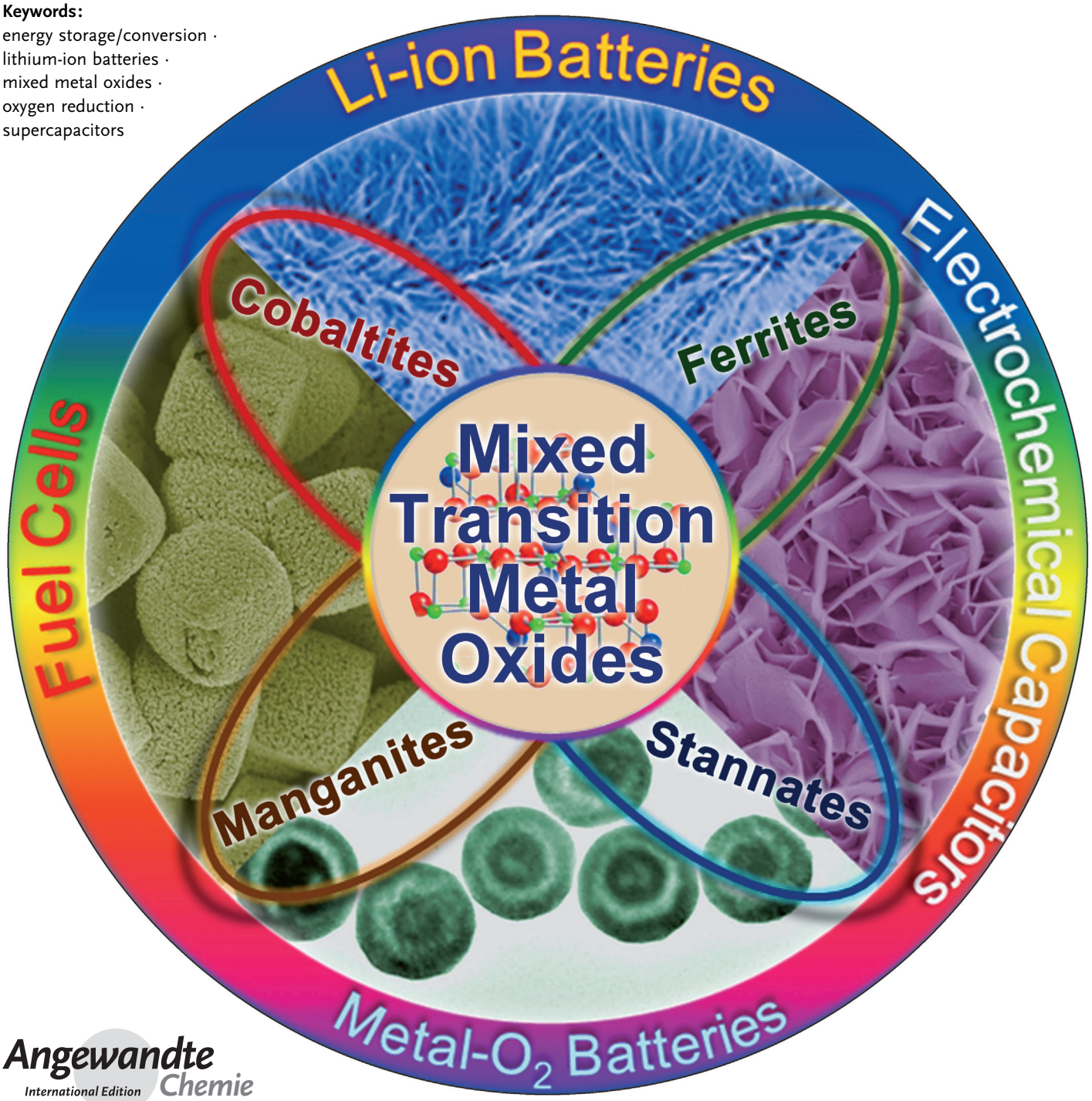

Angewandte International Edition Chemie

A promising family of mixed transition-metal oxides (MTMOs) (designated as $A_xB_{3-x}O_4$; A, B = Co, Ni, Zn, Mn, Fe, etc.) with stoichiometric or even non-stoichiometric compositions, typically in a spinel structure, has recently attracted increasing research interest worldwide. Benefiting from their remarkable electrochemical properties, these MTMOs will play significant roles for low-cost and environmentally friendly energy storage/conversion technologies. In this Review, we summarize recent research advances in the rational design and efficient synthesis of MTMOs with controlled shapes, sizes, compositions, and micro-/nanostructures, along with their applications as electrode materials for lithium-ion batteries and electrochemical capacitors, and efficient electrocatalysts for the oxygen reduction reaction in metal–air batteries and fuel cells. Some future trends and prospects to further develop advanced MTMOs for next-generation electrochemical energy storage/conversion systems are also presented.

From the Contents

1. Introduction

Clean and reliable energy supply is considered to be arguably one of the most significant concerns in the 21st century, which is ultimately related to our daily lives, global environment/economy, and human health. Although combustion-based energy technologies will continue to play a dominant role in meeting our energy needs in the near future, they come at a tremendous price, including a rapid increase in greenhouse gas emissions and long-lasting environmental pollution. The imminent shortage of fossil fuels and growing environmental concerns are pushing scientists and engineers to exploit sustainable, clean, and highly efficient technologies to supply and store energy.[1–4] In this regard, various electrochemical energy storage/conversion systems, such as lithium-ion batteries (LIBs), electrochemical capacitors (ECs), metal-O_2 batteries (MOBs, for example Zn-O_2 and Li-O_2 batteries), and fuel cells (FCs), are becoming more appealing than ever. All of them are termed collectively as electrochemical energy technologies, as they all rely on some common electrochemical principles. In the last few decades, these energy systems have witnessed their significant advances and great potential in many applications, including portable electronics, hybrid/pure electric vehicles, smart grids, and other rechargeable eco-friendly electronic devices.[1–8] More importantly, they convert chemical energy directly into electrical energy with high efficiency while causing little or no pollution. It should be stressed that LIBs, ECs, and MOBs are all electrochemical energy storage devices, whereas FCs are a typical electrochemical energy conversion system. Unfortunately, the widespread commercialization of these innovative electrochemical energy technologies is still greatly hampered by their high cost, insufficient duration, and operability problems, which are ultimately related to severe materials challenges. Therefore, elaborate exploration and rational design of new materials that can lower the cost, increase the efficiency, and improve the durability will have a significant impact on making these promising energy technologies commercially viable.

Interestingly, the elegant combination of two simple low-cost transition-metal oxides (TMOs), or a TMO and a post-TMO, into spinel-like structures, leads to formation of mixed transition-metal oxides (MTMOs) (donated as $A_xB_{3-x}O_4$; A, B = Co, Ni, Zn, Mn, Fe, and so on) with stoichiometric or even non-stoichiometric compositions. The MTMOs discussed herein refer to single-phase ternary metal oxides with two different metal cations, rather than mixtures of two binary metal oxides. These MTMOs are emerging as promising electrode materials for both LIBs and ECs.[9–13] Their high electrochemical activities owing to the complex chemical compositions and their synergetic effects contribute to the exceptionally high specific capacity/capacitance, which are typically 2–3 times higher than those of the graphite/carbon-based electrode materials. Furthermore, the presence of multiple valences of the cations in such spinel MTMOs systems is helpful to obtain the desirable electrochemical behavior of the electrocatalysts towards the oxygen reduction reaction (ORR) for high-performance MOBs and FCs by providing donor–acceptor chemisorption sites for the reversible adsorption of oxygen.[14–16] More significantly, these MTMOs usually exhibit higher electrical conductivity than simple TMOs owing to the relatively low activation energy for electron transfer between cations.[10,17,18]

It is well established that many characteristics of functional materials, such as composition, crystalline phase, structural and morphological features, and the sur-/interface properties between the electrode and electrolyte, would greatly influence the performance of these unique MTMOs

[*] Prof. Y. Xie
Hefei National Laboratory for Physical Sciences at the Microscale, University of Science & Technology of China
Hefei, Anhui 230026 (P.R. China)
E-mail: yxie@ustc.edu.cn
Dr. C. Z. Yuan,[+] H. B. Wu,[+] Prof. X. W. Lou
School of Chemical and Biomedical Engineering, Nanyang Technological University
62 Nanyang Drive, Singapore, 637459 (Singapore)
E-mail: xwlou@ntu.edu.sg
Homepage: http://www.ntu.edu.sg/home/xwlou/
[+] These authors contributed equally to this work.

in electrochemical energy storage/conversion applications.[14,19–27] There is thereby an urgent need but it is still a significant challenge to rationally design and delicately tailor the electroactive MTMOs for advanced LIBs, ECs, MOBs, and FCs. Of particular note, the spinel structure is one origin of the variety of interesting physical and chemical properties of a large number of functional MTMOs. Various cations with more than one oxidation state can be accommodated and distributed within the available octahedral and tetrahedral sites of the close-packed oxygen atoms,[26] which renders interesting and highly tunable properties. Furthermore, the performance of these electrochemical energy storage/conversion devices depends highly on the development of advanced electrode materials with excellent electrochemical properties, and the smart design of architectures for the MTMOs-based electrodes. The combination of these two aspects could realize superior ion transport, rapid electrode kinetics, high structural stability, and appealing electroactive sur-/interface between the electrode and electrolyte.

In this Review, we mainly address the topic on the design and controllable synthesis of these intriguing MTMOs for high-performance electrochemical energy storage/conversion technologies. To make it a feasible task, the scope of this Review focuses on four types of important electrochemical energy storage/conversion devices that might benefit from the use of MTMOs, namely LIBs, ECs, MOBs, and FCs. In Section 2, we will provide an overview of the applications of MTMOs for the above-mentioned electrochemical devices. The advantages and limitations will be discussed, and the impacts of structural/compositional engineering are also highlighted. In Section 3, the synthesis and electrochemical performance of diverse MTMOs are extensively reviewed, categorized based on the main metal oxides in their chemical compositions. Special emphasis is given to the excellent electrochemical properties of some advanced MTMOs-based materials, which originate from the advantageous compositional and structural features. In Section 4, we offer some personal prospects in the aim to shed some light on the further development of advanced MTMOs for next-generation electrochemical energy storage/conversion technologies.

2. Smart MTMO Architectures for Electrochemical Energy Storage and Conversion

2.1. Electrodes for Advanced LIBs and ECs

As two major devices for electric energy storage, LIBs and ECs have attracted worldwide interest, because of their vital role as the dominant power sources for portable electronics, and the great potential to power electric vehicles and for large-scale electric grids. In spite of their different definitions, both of them, in nature, belong to electrochemical energy storage devices, and have several similarities in configuration with a negative electrode (anode), an aqueous/non-aqueous/solid electrolyte, and a positive electrode (cathode).[1,5,20] In principle, the energy storage in these electrochemical cells depends on the reversible electrochemical reactions/charge storage in the electrode materials. During the electrochemical processes, the ions shuttle between the electrodes through the electrolytes, while the electrons flow through the external circuit. As anode materials for LIBs, MTMOs typically store lithium by the conversion reaction, which results in the reversible formation of metallic clusters embedded in a Li_2O matrix.[3] When applied as electrode materials for ECs, the charge storage in MTMO electrodes mainly comes from the pseudocapacitance, which originates from the fast redox reactions on the surface.[4]

To achieve the highly efficient energy storage, both of the two devices should be able to store and release large amount of electric energy at high rates. However, this would not be achievable without an elegant design of appropriate electrode materials. Accordingly, spinel MTMOs composed of two TMOs, or a TMO and a post-TMO, have aroused widespread attention as appealing potential electrodes for next-generation LIBs and ECs, because of the ease of large-scale synthesis, low cost, and remarkable electrochemical performance. Their rich redox reactions involving different ions contribute to high specific capacitance/capacity an order of magnitude beyond those of conventional carbon/graphite-based candidates.[5,9–13,19] The formation of mixed valence states at these multi-metal centers in the spinel MTMOs, even those with non-stoichiometric compositions, renders the desirable electronic conductivity for efficient energy storage, owing to the possible hopping processes[10,17,18] and/or defect effect mechanisms.[28,29] Moreover, the electrochemical energy storage of these unique MTMOs differs from simple

Xiong Wen (David) Lou was born in Zhejiang, PR China, in 1978. He received his BEng (1st class honors, 2002) and MEng (2004) degrees from the National University of Singapore. He obtained his PhD in chemical engineering from Cornell University in 2008. He is currently an Associate Professor in Nanyang Technological University. His current research is focused on design and synthesis of novel nanostructured materials for different applications in lithium-ion batteries, supercapacitors, electrocatalysis, and photocatalysis.

Yi Xie received her BS in Xiamen University (1988) and Ph. D at University of Science and Technology of China (1996). She is now a Principal Investigator (PI) of the Department of Nanomaterials and Nanochemistry, Hefei National Laboratory for Physical Sciences at Microscale and a full professor of Department of Chemistry, University of Science and Technology of China. She was appointed as the Cheung Kong Scholar Professor of inorganic chemistry in 2000. Her research interests are four major frontiers: nanotechnology, solid-state chemistry, energy science, and theoretical physics.

TMOs owing to the different compositions, including element species and ratios. However, the cyclability of the MTMOs-based LIBs and ECs is still not satisfactory when compared to the commercial standards of LIBs (400–1200 cycles) and ECs (not less than 10000 cycles), which is possibly due to the sluggish electronic/ionic transport, and the poor structural stability that might fail to sustain large volume change and lead to serious aggregation.[5] The undesirable rate performance of LIBs and modest energy density of ECs must also be further taken into serious consideration for their practical use. To well circumvent these issues, it is thus important and logical to carefully exploit and develop advanced MTMO electrodes with rapid ionic transport, fast electrode kinetics, and desirable structural stability by purposeful design and optimization of the compositions/components, crystallinity, architectures, and electrode/electrolyte interfaces of the striking MTMOs for much more efficient energy storage.

The recent remarkable progress in LIB and EC technologies has greatly benefited from moving conventional to nanostructured electrodes. In general, when the unique MTMO structures are made into intriguing nano-architectures, particularly with large specific surface area (SSA) and proper pore size distribution (PSD), several attractive features favoring the efficient energy storage would be manifested for advanced LIBs and ECs as follows:[3,7]

1) better accommodation of the strain during Li^+ insertion/removal, thus enhancing the cycling performance;
2) improved reactivity triggering new reactions that are impossible for bulk materials;
3) large electrode/electrolyte contact surface, resulting in sufficient electroactive sites;
4) short path length for electronic transport, permitting operation with low electrical conductivity or at high power; and
5) convenient diffusion paths for ionic transport, which is due to the desirable mesoporosity.

It is with these appealing perspectives that MTMO nanoarchitectures have been extensively pursued for improving the electrochemical performance of LIBs and ECs. In the past decade, numerous spinel MTMOs with diverse nanostructures, including nanofibers (NFs),[12] nanotubes (NTs),[30,31] nanowires (NWs),[32–36] nanorods (NRs),[37] nanoneedles,[38] nanosheets (NSs),[38–40] nanoparticles (NPs),[41–43] nanoaerogels,[10,44,45] nanoplates,[46] and nano-octahedrons,[47,48] have been extensively synthesized and applied as excellent electrode materials for high-performance LIBs and ECs.

Nevertheless, for conventional nanostructured MTMOs as mentioned above, some problematic disadvantages cannot be overlooked. For example, the large external surface area increases the undesirable electrode/electrolyte reactions, leading to an increase in solid-electrolyte interfacial (SEI) layer area. Other flaws include obvious self-discharge, large capacity/capacitance loss, inferior cycle life, low packing density leading to lower volumetric energy density, and so on.[3,7] These drawbacks can be largely addressed by the higher-level organized structures, that is, elegant hierarchical micro-/nanostructures, where the particles are typically of micro-/submicrometer dimensions but internally consist of nano-building blocks and/or nano-domains.[3,49,50] The unique hierarchical micro-/nanostructures, as secondary superstructures, could offer the exceptional advantages of both nanometer-sized building blocks/nano-domains (NPs, NWs, NSs, and so on) and micro-/submicrometer-sized assemblies (for example, urchin-like microspheres,[51–53] mesoporous microspheres,[54–57] core–shell mesoporous microspheres,[58] double-shelled hollow microcubes,[9] ball-in-ball hollow microspheres,[11] flower-like superstructures[59]). In particular, when hierarchical hollow MTMO micro-/nanostructures, especially with complex shell and interior structures, are well constructed, remarkable electrochemical performance could be highly anticipated both for advanced LIBs and ECs, owing to the large SSA, short ionic and electronic diffusion paths, and desirable hierarchical porosity (that is, meso- and macroporosity).[9,11,54–58] The integration of the concept of hierarchical hollow micro-/nanostructures with electroactive MTMOs provides a fascinating avenue to produce next-generation electrode materials with superior advantages over conventional bulk and/or solid nanostructured materials. The large SSA of the hollow MTMOs, particularly with finely controlled shell thickness and internal void size, endows many electroactive sites and large electrode/electrolyte interfaces for high ion flux across and/or adsorption/desorption on the surfaces and/or interfaces.[9,11,13,50]

The hierarchical porosity might provide multiple functionalities to enhance the electrochemical performance. Specifically, the mesopores possess the ability to hold the electrolyte and prevent it from over-flooding under capillary force. Meanwhile, the macropores of interior cavities, serving as the "ion-buffering reservoirs", minimize the diffusion distance to the interior surface, which may accelerate the kinetic process of the ion diffusion in the electrode. Furthermore, the permeable thin shells greatly afford reduced paths for both ion and electron diffusion, leading to even better rate capability. Especially for LIBs, the hierarchical hollow interior also provides extra free space for alleviating the structural strain and accommodating the large volume variation associated with repeated Li^+ ion insertion/extraction processes, giving rise to long-term stabilization.[13,50] For the same reasons, multi-shelled hierarchical hollow micro-/nanostructures might manifest even better performance for advanced LIBs and ECs.[9,11]

To further improve the performance of MTMOs, many MTMO-based hybrid materials have been extensively prepared and studied. The MTMO-based hybrid materials mentioned here mainly refer to the composites consisting of MTMOs and various carbonaceous materials. Several functional carbon materials (for example, amorphous carbon,[55,60,61] ordered mesoporous carbon materials (OMCs),[62,63] carbon nanotubes (CNTs),[64,65] and graphene nanosheets (GNs)[66–68]) with desirable electrical conductivity, large SSA, and proper PSD are widely used as effective matrixes to support, disperse, or encapsulate the MTMOs. The two components of these MTMO-based hybrid materials are well-constructed with two or more levels in a hierarchical structure with the ultimate aim of improving the electrical conductivity, enhancing naked electroactive sites, buffering the volume changes, and preventing interparticle agglomer-

ation.[55,60–62,64–67,69] For example, for electrode materials of LIBs, carbon nanocoating has been commonly used as an elastic layer for effectively buffering the volumetric changes and preventing the pulverization of MTMO electrodes during the insertion/extraction of Li^+ ions, and also a conductive additive for enhancing the electrical conductivity, resulting in high specific capacity, good cyclability, and rate performance. With regard to the ECs application, such hybrids combine the carbon-based electric double layer system and the MTMO-based Faradaic pseudocapacitive system, which can utilize both the fast and reversible double-layer capacitance at the electrode/electrolyte interfaces and the Faradaic capacitance originated from the pesudocapacitive MTMO species. In virtue of the synergetic effects of the two distinct compositions, the energy density of the resultant carbon-MTMO hybrid materials can be undoubtedly optimized without deteriorating their intrinsic high power capability, which is the most critical aspect in the development and commercial application of the advanced ECs. However, it is highly desirable but challenging to design and synthesize unique MTMO-based hybrids with hierarchical structures by controllable, simple and easy scale-up approaches, thus to effectively tailor the physical/chemical properties of these electroactive MTMOs for high-performance LIBs and ECs.

Along with conventional electrode materials in the form of powder or particles, self-supported binder-free MTMOs[1,5,38–40,70–72] have also drawn considerable attention. These unique MTMO nanostructures are directly aligned on conductive substrates, such as Ni foam,[38–40,72] Ti foil,[38,40] stainless-steel foil,[40] flexible graphite paper,[40] Cu foil,[71] carbon cloth,[70] and so on, and then applied as integrated electrodes without adding any extra binders and conductive additives. Thus the electrode fabrication process could be simplified and the cost could be reduced as well. Of particular interest, when some intriguing ordered array architectures are efficiently constructed on these low-cost current collectors with good adhesion, remarkable enhancement in electrochemical performance could be realized by the advantageous structural features. Specifically, the arrays directly grown on conductive substrates have outstanding electrical conductivity because each array nano-building block sticks tightly to the current collector to form very good adhesion and electrical contact, building up an expressway for electric charge transfer. The three-dimensional (3D) configuration of the unique self-supported arrays ensures the porous textures and open space between neighboring array nano-building blocks, thus greatly enhancing the electrode/electrolyte contact area. It provides ideal conditions for facile penetration of the electrolyte and accommodation of the strain induced by the volume change during electrochemical reactions, thus bringing higher efficiency for the electrochemical energy storage.[1,5] Thereby, a wide variety of self-supported MTMO nanostructures[38–40,70–72] have been rationally designed and extensively explored as next-generation competitive candidates for advanced LIBs and ECs, owing to the structural superiority mentioned above.

2.2. Electrocatalysts for the Oxygen Reduction Reaction (ORR)

The cathodic ORR has been one focus of electrochemistry in the past decades owing to its significance to numerous energy storage/conversion technologies, including MOBs (such as, Zn-O_2, Li-O_2 batteries) and FCs.[14–16,73] For these electrochemical devices, the energy storage/conversion relies on the controllable oxidation of metals (for MOBs) or fuel molecules, such as hydrogen and methanol (for FCs). Meanwhile oxygen is reduced with the assistance of proper electrocatalysts. During the ORR process, molecular oxygen in the cathode will receive electrons from the counter metal electrode to complete the electrochemical reaction, and finally electric energy is generated. It is well-accepted that the ORR is a complicated condition-sensitive multi-step reaction, as the ORR pathway depends on not only the adsorption configuration of molecular oxygen, which is related to the crystallographic structure of electrocatalyst itself (geometrical effect) and the binding energy (chemical effect) between oxygen and catalytic sites, but also the interaction between molecular oxygen and catalytic sites.[14,74,75] Owing to its sluggish kinetics, the ORR traditionally requires the exclusive use of Pt-based electrocatalysts. Unfortunately, the intriguing electroactivity of Pt-based electrocatalysts commonly comes at the expense of high cost and limited stability, which greatly motivates the design and screening of innovative catalysts with higher durability and much lower cost to replace Pt for efficient electrochemical reduction of O_2.[14–16,73–76]

Some emerging alternative electrocatalysts investigated for the ORR are multi-valence mixed oxides of transition metals with a spinel structure, which is an important class of MTMOs with appealing ORR catalytic activity in alkaline aqueous and/or non-aqueous media.[14–16,73–75] The advantages of using these MTMOs as electrocatalysts for the ORR are associated with their desirable activity, widespread availability, low cost, thermodynamic stability, low electrical resistance, and environmental friendliness.[14–16,73–75] The presence of mixed valences in the same type of cation in such spinel MTMOs is highly beneficial for the ORR by providing donor–acceptor chemisorption sites for the reversible adsorption of oxygen.[14] Furthermore, these MTMOs exhibit relatively high electrical conductivity owing to the electron transfer between cations with different valences, which greatly affects the strength of the surface-intermediate bonds and depends on the chemical structure of the surface.[14,17] It should be pointed out that the nanometer-scale distribution of electrocatalyst centers on the electrode surface is also a predominant factor for high ORR electrocatalytic activity. This furthermore requires the need for fine design and tailoring of their geometrical morphologies, which are directly related to the actual surface area or electroactive site density.[14] This fact consequently requires the employment of nanoparticulate MTMOs with rich electroacitve sites as the attractive electrocatalysts for the ORR. Furthermore, besides efficient adjustments of the inherent electrical conductivity of the MTMOs, fast electron transport achieved by designing proper nanostructure and composition is also critical to obtain good electrocatalytic activity of these MTMOs. These

nanoscale MTMOs embedded in a conductive matrix, especially some carbon materials with high electrical conductivity, high SSA, and suitable functional groups on carbon surfaces,[15,73,76,77] appear to be promising candidates for an efficient ORR. As a result, delicate optimization of particle size, composition, carbon matrix, and also innovative processing and fabrication methodologies is likely to play critical roles in achieving high electrocatalytic activity of O_2 reduction.

All in all, rational design of surface structure and conductivity of the MTMO electrocatalyts through cationic substitution and coupling with carbonaceous matrix with large SSA and good electrical conductivity should greatly benefit the rapid development of advanced MTMO electrocatalysts for an efficient ORR. Moreover, the synergetic chemical coupling effects between nanoscale MTMO NPs and carbonaceous supports would provide a major boost for MOBs and FCs towards their potential commercialization in future.

3. Controllable Synthesis of MTMOs and Their Energy-Related Applications

Similar to simple metal oxides, a wide variety of synthetic methods has been applied to fabricate MTMOs. Of particular note, solution-based syntheses, such as hydrothermal,[15,40] solvothermal,[11,31] and some room-temperature methods,[9,16] usually coupled with post annealing, have been widely adopted to prepare MTMOs with diverse compositions and nanostructures. The thermal treatment typically transforms the precursors obtained from the solution synthesis into the desired MTMOs. Re-crystallization, volume change, and possibly gas release would take place during the annealing process, which commonly result in the formation of high porosity and even hollow structures.[9,11] These structural features are highly beneficial for electrochemical applications as discussed earlier. Alternatively, such highly porous and/or hollow structures can also be obtained by the interconnection of nanoscale building blocks (for example, NSs)[39,40] and hard-templating methods.[25,31] The synthesis, structure, and electrochemical performance of various MTMOs will be thoroughly reviewed in this section. Considering the critical effects of the chemical composition on their physical/chemical properties, these MTMOs would be categorized based on the dominant metallic species in their compositions.

3.1. Cobaltites

Co_3O_4 has been widely studied as an interesting anode material for LIBs owing to its high reversible capacity and easy preparation in comparison to other cobalt oxides/nitride, such as CoO, Co_2O_3, and CoN.[78,79] However, cobalt species are somewhat toxic and expensive. Therefore, the worthwhile efforts have been made towards partially replacing the Co in Co_3O_4 by much cheaper and more eco-friendly alternative elements without sacrificing the good electrochemical performance. As a result, the spinel compounds $M_xCo_{3-x}O_4$ (M = Ni, Mn, Fe, Cu, Zn, etc.) possessing isostructural nature to Co_3O_4 are formed, and can reversibly react with lithium mainly by the conversion reaction[25,27,56,57,61,71,80–82] coupled with possible alloying/de-alloying mechanism (only for Zn).[30,70,83,84] Such a family of $M_xCo_{3-x}O_4$ is very promising as competitive anode materials with respect to practical LIB applications.

The electrochemical lithium storage properties of $FeCo_2O_4$ and $MgCo_2O_4$ have been investigated by Chowdari's group.[27] Unlike Fe and Co ions, the Mg ion is not electroactive towards Li, whereas the electroactive Fe species is found to be a better counter ion than the Mg ion. Chowdari and co-workers also investigated $CuCo_2O_4$ as an anode material for LIBs. The reported nanocrystalline $CuCo_2O_4$ electrode keeps a charge capacity of 755 $mA\,h\,g^{-1}$ at the 20th cycle under a current density of 60 $mA\,g^{-1}$.[82] Furthermore, a well-ordered mesoporous crystalline $CuCo_2O_4$ has been synthesized by Wen and co-workers[25] by a nanocasting strategy using the KIT-6 mesoporous silica as the hard template, and delivers an initial discharge capacity of 1564 $mA\,h\,g^{-1}$ and a reversible capacity of 900 $mA\,h\,g^{-1}$ after the 6th cycle at 60 $mA\,g^{-1}$. Preliminary results on the lithium storage properties of $NiCo_2O_4$[80] and $MnCo_2O_4$[81] were reported by Tirado's group, and recently they have established the reaction mechanism of the Li-$NiCo_2O_4$ system.[80] More interestingly, Liu and co-workers developed a mild and cost-effective solution route to directly grow $NiCo_2O_4$ NR arrays on a Cu substrate.[71] With well-aligned 1D NR microstructure and high electrical conductivity, the self-supported array electrode manifests high specific capacity, excellent cycling stability (a high reversible capacity of about 830 $mA\,h\,g^{-1}$ achieved after 30 cycles at 0.5 C) and high rate capability (787 and 127 $mA\,h\,g^{-1}$ at 1 C and 110 C, respectively). Yang et al.[61] obtained a $NiCo_2O_4$/C hybrid material by a facile hydrothermal method followed by calcination. Owing to the high dispersion of $NiCo_2O_4$ NPs within the amorphous carbon matrix and the good interfacial affinity between the two components, the hybrid material displays outstanding electrochemical activity with an initial Coulombic efficiency of 79.2 %, large reversible capacity of 914.5 $mA\,h\,g^{-1}$, and desirable capacity retention of 78.3 % upon 50 cycles at 40 $mA\,g^{-1}$. Furthermore, non-stoichiometric spinel $Mn_{1.5}Co_{1.5}O_4$ core–shell microspheres[58] were synthesized by a urea-assisted solvothermal route followed by pyrolysis of the carbonate precursor. Such core–shell microspheres exhibit a high capacity of 618 $mA\,h\,g^{-1}$ at 400 $mA\,g^{-1}$ even after 300 discharge–charge cycles when evaluated as an anode material, which is attributed to the appropriate pore size and unique core–shell structure.

From the above discussion, it is clear that the particle size, morphology, composition, pore structure, micro-/nanostructure, and the counter cation in the spinel Co-based compounds play significant roles on the attainable reversible capacity, rate capability, and long-term cyclability. It is noteworthy that, among these Co-based MTMO anodes, $ZnCo_2O_4$, in which bivalent Zn-ions occupy the tetrahedral sites in the spinel structure and trivalent Co-ions occupy the octahedral sites, is of significant interest. Apart from the conversion reaction between Zn/Co species and Li, the alloying reaction between Zn and Li could contribute to

additional lithium storage capacity of $ZnCo_2O_4$.[30,70,83,84] Interestingly, a unique hierarchical 3D $ZnCo_2O_4$ NWs arrays/carbon cloth anode (Figure 1a) has been synthesized by using a facile hydrothermal route, and directly applied as the self-supported anode for LIBs.[70] The integrated electrode could be readily rolled up repeatedly with a tweezer (Figure 1b), demonstrating the possibility for further flexible device applications. As observed in Figure 1c,d, each $ZnCo_2O_4$ NW array/carbon composite fiber possesses uniform diameter, and consists of numerous highly ordered 3D $ZnCo_2O_4$ NW arrays densely grown on each individual carbon microfiber. Notably, the $ZnCo_2O_4$ NW with a diameter of 80–100 nm is composed of many even smaller NPs and exhibits a typical mesoporous structure (Figure 1e). Benefiting from these advanced structural features, this binder-free anode demonstrates excellent reversible capacity, exceptional cycling stability (Figure 1f), and remarkable rate performance (Figure 1g). No obvious decay in capacity is found for the binder-free anode and the capacity remains around 1200 mA h g^{-1} even after 160 cycles at a current density of 200 mA g^{-1}. During cycling, the high Coulombic efficiency of 99% (Figure 1f) further indicates the remarkable electrochemical reversibility during the lithium insertion and extraction reactions. The appealing electrochemical behaviors of such a self-supported electrode can be attributed to the synergetic effects of the $ZnCo_2O_4$ NW arrays and conductive carbon cloth backbone (Figure 1h). Considering that no ancillary materials such as polymer binder and carbon black are used in the work, the present hierarchical $ZnCo_2O_4$ NW arrays/carbon cloth is a promising anode candidate for high-performance flexible LIBs.

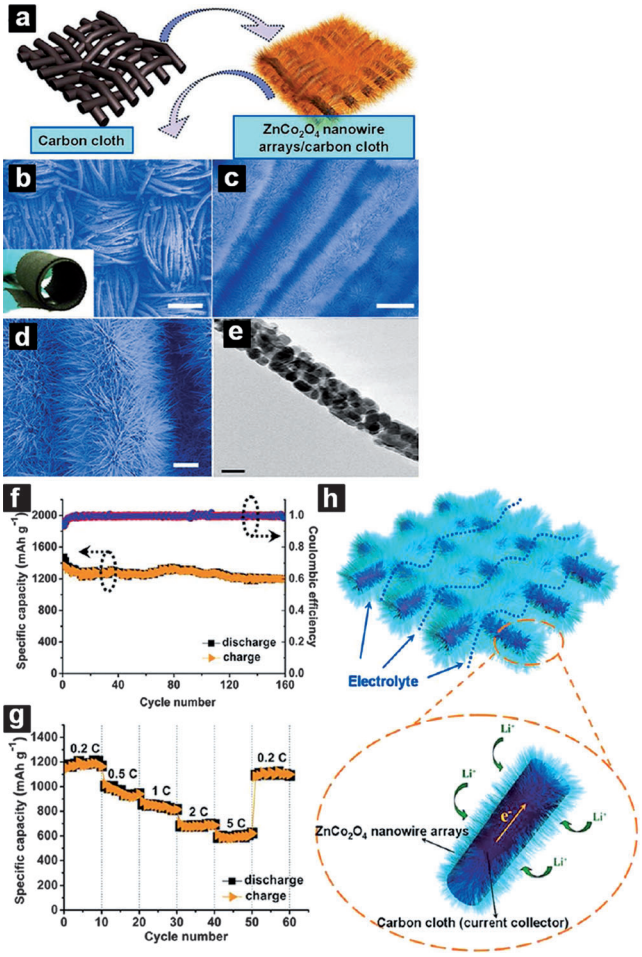

Figure 1. a) The synthesis of flexible 3D $ZnCo_2O_4$ NW array/carbon cloth. b)–d) Field emission SEM (FESEM) images of the $ZnCo_2O_4$ NW arrays grown on carbon cloth and e) TEM image of a single $ZnCo_2O_4$ NW. Inset in panel (b) shows an image of product rolled up with a tweezer, suggesting very good flexibility. Scale bars: b) 200 μm, c) 20 μm, d) 5 μm, e) 50 nm. f) Cycling performance of the $ZnCo_2O_4$ NW array/carbon cloth electrode. g) Capacity versus cycle number at different charging rates. h) Representation and operating principles of rechargeable LIBs based on the $ZnCo_2O_4$ NW array/carbon cloth. Panels (a–h) are reproduced with permission:[70] Copyright 2012, ACS.

Apart from the appealing application in LIBs, the low-cost Co-based MTMOs also demonstrate excellent electrochemical performance as typical pseudocapacitive materials for advanced ECs. Among these cobaltites, the spinel $NiCo_2O_4$ with a general formula of $Co^{2+}_{1-x}Co^{3+}_x[Co^{3+}Ni^{2+}_xNi^{3+}_{1-x}]O_4$ $(0<x<1)$, where the cations within the square brackets are in octahedral sites and the outside cations occupy the tetrahedral sites, has drawn worldwide attention for advanced EC application. It is due to the presence of mixed valences of the same cation in such cobaltite spinel system that $NiCo_2O_4$ possesses at least two orders of magnitude higher electrical conductivity than monometallic nickel and cobalt oxides. The conductivity is documented as 62 S cm^{-1} for single crystal $NiCo_2O_4$ nanoplates at room temperature,[17] and 0.6 S cm^{-1} for polycrystalline $NiCo_2O_4$ film at 300 °C.[18] Furthermore, rich redox reactions originating from both nickel and cobalt cations render its promising electrochemical properties as an alternative pseudocapacitive electrode material.

More specifically, Hu et al.[10] reported the first successful preparation of $NiCo_2O_4$ aerogels, by a simple epoxide-driven sol–gel process, and their performance in ECs. The typical mesoporous nature, manifested as the inter-connection of NPs, of the resulting $NiCo_2O_4$ aerogels with enhanced crystallinity is clearly displayed after calcination at 200 °C (Figure 2a–e). Also, the PSD of the aerogels falls in the optimal narrow size range of 2–5 nm (Figure 2f) that is favored for EC application.[85,86] Accordingly, the coexistence of nickel and cobalt cations, mesoporous characteristics, and nanocrystalline nature are responsible for the outstanding electrochemical capacitive properties. An improved reversibility of the redox characteristics of the resultant $NiCo_2O_4$ after calcination at 200 °C is clearly observed (Figure 2g), which is due to the enhanced crystallinity. Impressively, the unique mesoporous $NiCo_2O_4$ aerogels deliver an extremely high specific capacitance (SC) of 1400 F g^{-1} after 650-cycle activation (Figure 2h). The decay in the SC, based on this maximum value after a 2000-cycle test, is quite insignificant, revealing the desirable stability of the $NiCo_2O_4$ material. Following this pioneering work, various $NiCo_2O_4$ nanostructures, including platelet-like NPs,[87] coral-like porous crystals,[41] ordered mesoporous particles,[88] 1D porous NWs,[33,35,36] and some urchin-like micro-/nano-structures,[51–53] have been fabricated extensively as attractive

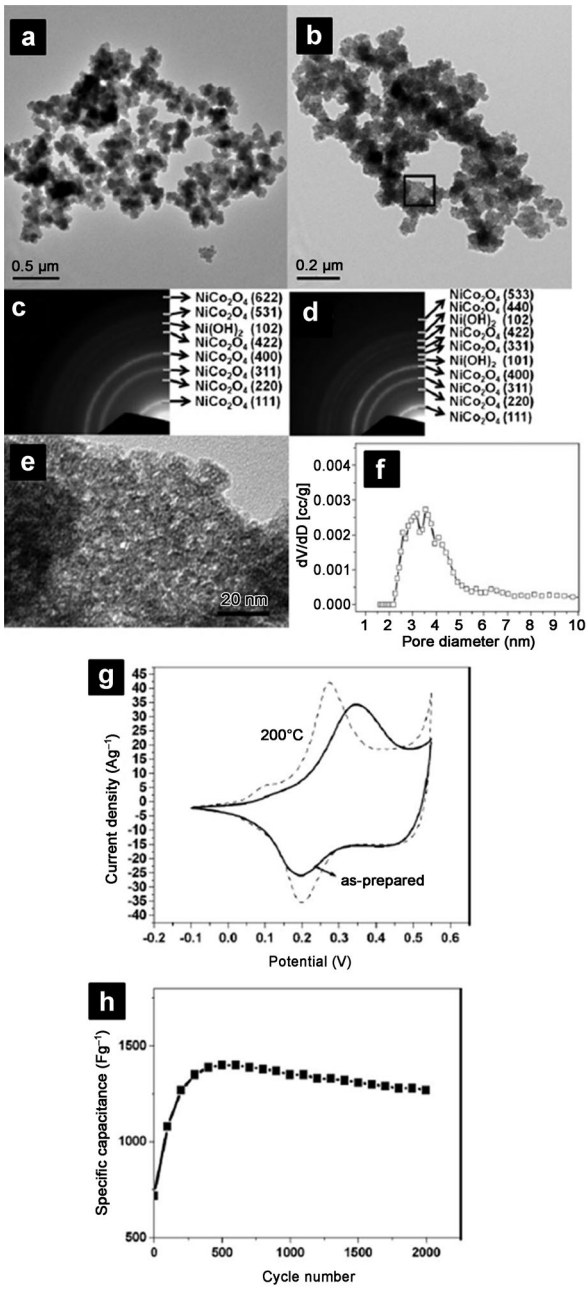

Figure 2. a), b) TEM images and c), d) selected-area electron diffraction (SAED) patterns of a), c) as-prepared $NiCo_2O_4$ and b), d) the $NiCo_2O_4$ obtained after calcination at 200 °C. e) High-magnification TEM image, f) pore size distribution, g) CV curves and h) cycling performance of the $NiCo_2O_4$ obtained after calcination at 200 °C. Panels (a–h) are reproduced with permission:[10] Copyright 2010, Wiley.

pseudocapacitive materials for high-performance ECs. Moreover, significant enhancement is still possible by improving the SSA and electrical conductivity of the $NiCo_2O_4$ electrode, thus further enhancing its electrochemical utilization. This goal can be commonly achieved by using mesoporous or high-SSA carbon matrix with high electrical conductivity to disperse and/or host the nanosized $NiCo_2O_4$ phase. The tailored hybrid architectures enable nanosized $NiCo_2O_4$ well exposed to the electrolyte, and easy transport of ions and electrons within such hybrid electrodes. As a consequence, various carbon supports, such as OMC,[62] CNTs,[64] carbon aerogel,[45] reduced graphene oxide (rGO),[89] and carbon fibers (CFs)[90] have been widely utilized to support and disperse the nanoscale $NiCo_2O_4$ with the ultimate aim to improve the electrochemical utilization and stability especially at high power output.

Interestingly, 1D NW hybrid materials composed of $NiCo_2O_4$ NRs (Figure 3a, b) or ultrathin porous NSs (Figure 3c, d) grown on CFs are fabricated through a facile

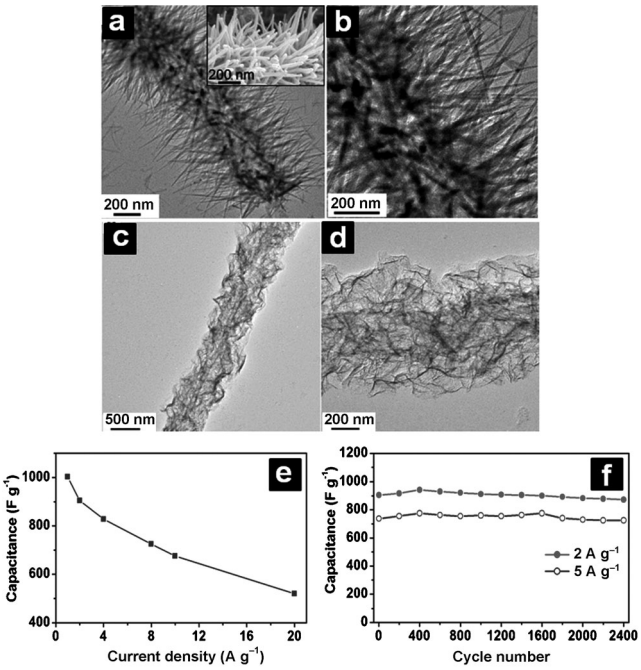

Figure 3. TEM images of a), b) $NiCo_2O_4$ NRs/CFs and c), d) $NiCo_2O_4$ NSs/CFs hybrids. The inset in (a) is an enlarged view of corresponding FESEM image. e) The calculated capacitance as a function of current density. f) The capacitance as a function of cycle number. Panels (c–f) are reproduced with permission:[90] Copyright 2013, Nature Publishing Group.

solution route combined with a post annealing treatment.[90] Owing to the ultrathin, large SSA, mesoporous and 2D features, the $NiCo_2O_4$ NSs/CNFs hybrid structure manifests an even better electrochemical capacitive performance than the $NiCo_2O_4$ NRs/CNFs material. Strikingly, the SCs of $NiCo_2O_4$ NSs/CNFs hybrid are as high as 1002, 905, 828, 725, 675, and 520 $F g^{-1}$ at high current densities of 1, 2, 4, 8, 10, and 20 $A g^{-1}$, respectively (Figure 3e). A low SC loss of only about 3.6% is observed at 2 $A g^{-1}$ over 2400 cycles. Even with a higher current density of 5 $A g^{-1}$, the SC degradation is still as low as 7.25% (Figure 3f).

Unfortunately, most of the $NiCo_2O_4$ materials mentioned above are commonly pelletized in a paste electrode for electrochemical evaluation. A large portion of surface is thus left as "inert surface", which is not in contact with the electrolyte ions and thus cannot participate in the Faradaic reactions for efficient energy storage, especially at high rates. To well address the issues mentioned above, an emerging

novel concept is to grow electroactive $NiCo_2O_4$ nanostructures on conductive current collectors, which are directly used as integrated electrodes for advanced ECs. Mesoporous $NiCo_2O_4$ nanoarchitectures (for example, NSs, nanoneedles) supported upon various conductive substrates[38–40,91,92] have been exploited by electrodeposition, chemical bath deposition, simple solution routes, and so on.

We have successfully developed a simple yet general solution method combined with a post-annealing treatment to directly grow interconnected mesoporous $NiCo_2O_4$ NSs on various conductive substrates (for example, Ni foam, Ti foil, stainless-steel foil, and flexible graphite paper) with robust adhesion as binder- and conductive-agent-free electrodes for ECs.[40] The $NiCo_2O_4$ NSs/nickel foam integrated electrode (Figure 4a–c) with a mass loading of 1.2 mg cm^{-2} exhibits very high SCs of 2.09 F cm^{-2} at 8.5 mA cm^{-2}, and even 1.28 F cm^{-2} at a large current density of 25 mA cm^{-2} (i.e., ~24 A g^{-1}), and excellent cycling stability (SC loss of ca. 6.7% at 8.5 mA cm^{-2}, and ca. 17% at 25 mA cm^{-2}) over 3000 continuous cycles (Figure 4d). Furthermore, single-crystalline nanoneedle arrays of $NiCo_2O_4$ on Ti foil (Figure 4e) or nickel foam (Figure 4f) can be grown through a simple solution method together with a post annealing treatment.[38] Thanks to the small diameter of nanoneedles and the well-defined array structure, the $NiCo_2O_4$ nanoneedle arrays/nickel foam electrode delivers a high areal SC of 1.01 F cm^{-2}, corresponding to a gravimetric SC of 1118.6 F g^{-1}, with a desirable SC retention of 89.4% after 2000 cycles at a current density of 6.56 mA cm^{-2} (Figure 4g). Furthermore, a facile two-step method, electrodeposition and subsequent calcination, has been developed for large-scale growth of ultrathin mesoporous $NiCo_2O_4$ NSs on Ni foam.[39] The as-prepared ultrathin mesoporous NSs are composed of 3–6 layers of $NiCo_2O_4$ atomic sheets, and possess numerous interparticle mesopores of 2–5 nm in size. The unique Ni foam-supported ultrathin mesoporous $NiCo_2O_4$ NSs (Figure 4h) promise fast electron and ion transport, large electroactive surface area, and excellent structural stability. As a result, superior pseudocapacitive performance (Figure 4i) is achieved with high SC and excellent cycling performance at large current densities.

Cobalt-based spinel MTMOs have been also investigated as efficient electrocatalysts for the ORR in alkaline aqueous and even non-aqueous electrolytes. Substituting Co in Co_3O_4 with Mn, Cu, and Ni has been extensively reported to lead to high electroactivity and stability for the ORR.[14,15,76,93,94] Despite these remarkable efforts, the Co-based MTMOs still exhibit a much lower mass activity compared with Pt-based materials. For instance, in 6 M KOH solution, a $MnCo_2O_4$-carbon black catalyst[94] with a loading of 14 mg cm^{-2} gives a current density of 300 mA cm^{-2} at 60 °C, while Pt/CNT/C with a loading of only 0.1 mg cm^{-2} gives a current density of 125 mA cm^{-2} at 25 °C.[94] Despite the low cost, there is a maximum acceptable loading of the electrocatalyst in the electrode owing to the resistivity in oxygen and electrolyte transport.[14] Therefore, it is highly desirable and necessary to develop spinel MTMO electrocatalysts with much improved gravimetric/volumetric catalytic activity.

In this regard, Dai et al.[15] synthesized a novel $MnCo_2O_4$/N-doped reduced graphene oxide (N-rGO) sheet hybrid as a highly efficient electrocatalyst for the ORR in KOH aqueous solution by taking advantage of the high electrocatalytic activity of $MnCo_2O_4$ compared to pure Co_3O_4 and the strong coupling with N-rGO. The nucleation and growth method results in covalent interaction between $MnCo_2O_4$ NPs and N-rGO sheets, giving rise to much higher activity and durability than the simple physical mixture of $MnCo_2O_4$ NPs and N-rGO (Figure 5a,b). Moreover, the Mn substitution mediates the size and phase of $MnCo_2O_4$, and increases the

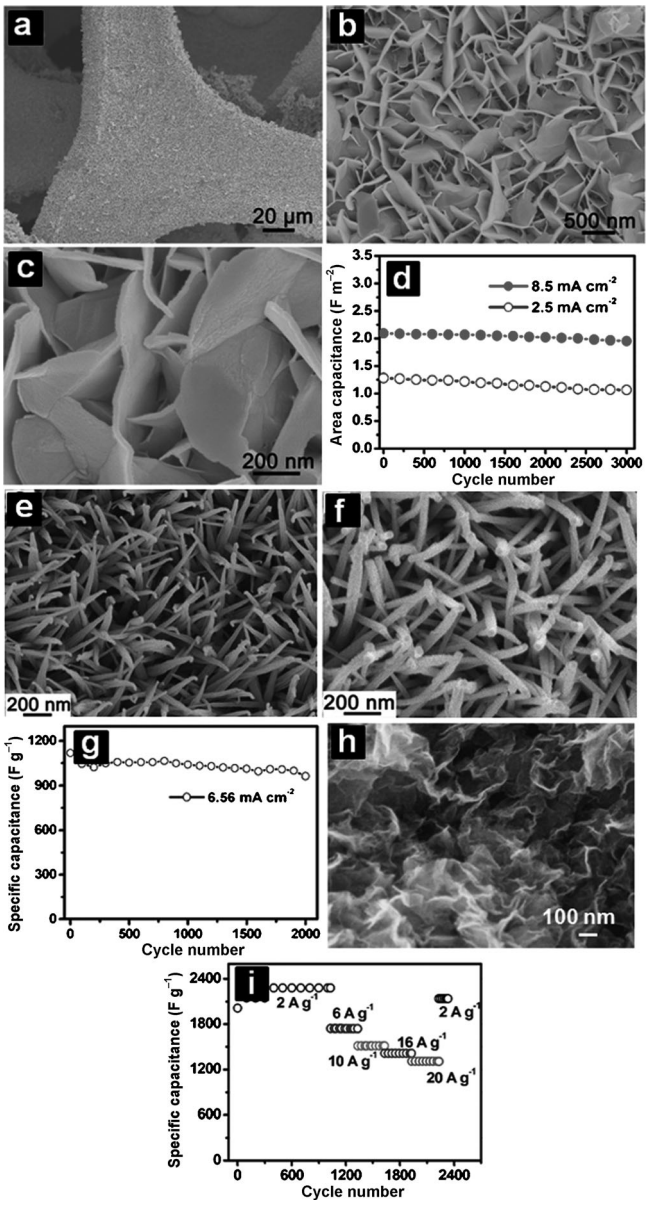

Figure 4. a)–c) Typical FESEM images and d) the SC as a function of cycle number of $NiCo_2O_4$ NSs on Ni foam. FESEM images of single-crystalline $NiCo_2O_4$ nanoneedle arrays supported on: e) Ni foam and f) Ti foil, and g) cycling performance of single-crystalline $NiCo_2O_4$ nanoneedle arrays supported on Ni foam. h) FESEM image and i) cycling performance of ultrathin $NiCo_2O_4$ NSs grown upon Ni foam. Panels (a–d) are reproduced with permission:[40] Copyright 2013, Wiley. Panels (e–g) are reproduced with permission:[38] Copyright 2012, RSC. Panels (h, i) are reproduced with permission:[39] Copyright 2012, Wiley.

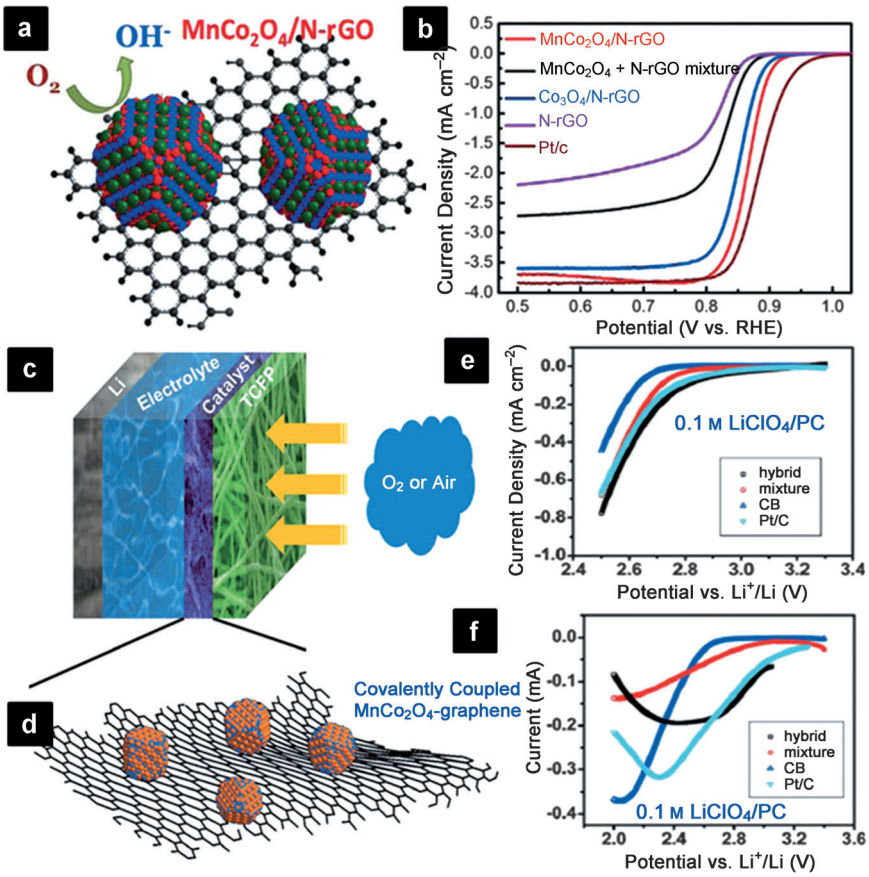

Figure 5. a) Representation of the structure of $MnCo_2O_4$/N-rGO hybrid; b) comparative rotating ring-disk electrode voltammograms of $MnCo_2O_4$/N-rGO hybrid and other electrocatalysts in O_2-saturated 1 M KOH at 5 $mV s^{-1}$ at 1600 rpm. c)–f) $MnCo_2O_4$-GN hybrid as a cathode catalyst for Li-O_2 batteries. c) Representation of the structures of the Li-O_2 cell catalyzed by the $MnCo_2O_4$-GN hybrid electrocatalyst (TCFP = Teflon-coated carbon fiber paper), and d) the $MnCo_2O_4$-GN hybrid material. ORR catalytic activity of the hybrid compared to control catalysts in 0.1 M $LiClO_4$/PC solution (PC = propylene carbonate). Catalysts were loaded on e) Teflon-coated carbon fiber papers and f) a glassy carbon electrode. Panels (a, b) are reproduced with permission:[15] Copyright 2012, ACS. Panels (c–f) are reproduced with permission:[76] Copyright 2012, RSC.

activity of catalytic sites of the hybrid materials, which eventually boosts the ORR activity compared with the pure Co_3O_4/N-rGO hybrid. With the same mass loading, the $MnCo_2O_4$/N-rGO hybrid can even outperform Pt/C in ORR current density at potential of < 0.75 V (vs. RHE) with stability superior to Pt/C, as shown in Figure 5b. More importantly, the rotating disk electrode measurements indicate that the ORR catalyzed by $MnCo_2O_4$/N-rGO is mainly through the $4e^-$ pathway.

Furthermore, Dai and co-workers[76] prepared $MnCo_2O_4$/GNs hybrid by a two-step solution method and employed the hybrid as the cathode electrocatalyst of the ORR for Li-O_2 batteries with a non-aqueous electrolyte (Figure 5c,d). The Li-O_2 cell with the hybrid electrocatalyst has similar low charge-discharge overpotentials as the Pt/C catalyzed cell, but with a much longer cycle life reported in a similar electrolyte at comparable gravimetric current densities. Owing to the strong electrochemical coupling between the GNs and the $MnCo_2O_4$ NPs in the hybrid, the electrocatalyst outperforms other metal oxide-based and carbon-based electrocatalysts under similar measurement conditions (Figure 5e,f), which makes it possible to realize Li-O_2 cells with high capacity, low overpotential, and good cycling stability.

3.2. Manganites

Manganese (Mn) is more environmentally benign, much cheaper (manganese is about 20 times less expensive than cobalt), and more abundant on earth compared to cobalt. Moreover, Mn-based negative electrodes (anodes) possess lower operating voltages (1.3–1.5 V for lithium extraction) compared to CoO_x (2.2–2.4 V).[95] As a consequence, LIBs with these Mn-based anodes can offer higher output voltage and higher energy density. In view of the above-mentioned considerable advantages, manganites of transition and/or post transition metals, that is, $M_xMn_{3-x}O_4$ (M = Co, Ni, and Zn),[9,11,22,34,42,46,56,95–98] are appealing high-capacity anodes for LIBs. Abu-Lebdeh et al.[22] presented a facile co-precipitation method to synthesize $CoMn_2O_4$, $NiMn_2O_4$, and $ZnMn_2O_4$. Among these spinel mixed-metal oxides, $ZnMn_2O_4$ shows significant improvement in the capacity retention over simple ZnO and Mn_2O_3, while $CoMn_2O_4$ and $NiMn_2O_4$ give either lower or more rapidly fading capacity, in contrast with $ZnMn_2O_4$. To enhance the electrochemical properties of $CoMn_2O_4$, we have synthesized novel double-shelled $CoMn_2O_4$ hollow microcubes with nanometer-sized building blocks (Figure 6a–e) by a facile co-precipitation and annealing method.[9] Owing to the heterogeneous contraction caused by non-equilibrium heat treatment (Figure 6a), the double-shelled $CoMn_2O_4$ hollow microcubes are obtained and exhibit a reversible capacity of about 830 $mA h g^{-1}$ at a current density of 200 $mA g^{-1}$, which remains as high as 624 $mA h g^{-1}$ after 50 cycles. The lithium storage properties of the double-shelled $CoMn_2O_4$ hollow microcubes are superior to that of the sub-micrometer-sized $CoMn_2O_4$ particles[22] and quasi-hollow $CoMn_2O_4$ microspheres.[56] Even at a high current density of 800 $mA g^{-1}$, a discharge capacity of 406 $mA h g^{-1}$ is retained after 50 cycles. The remarkable electrochemical performance (Figure 6f) of the resultant $CoMn_2O_4$ material can be attributed to the following two aspects: 1) the nanometer-sized subunits make the conversion reaction more feasible, and allow the reversible formation/dissolution of polymeric gel-like film at the surface of the electroactive material, both of which contribute

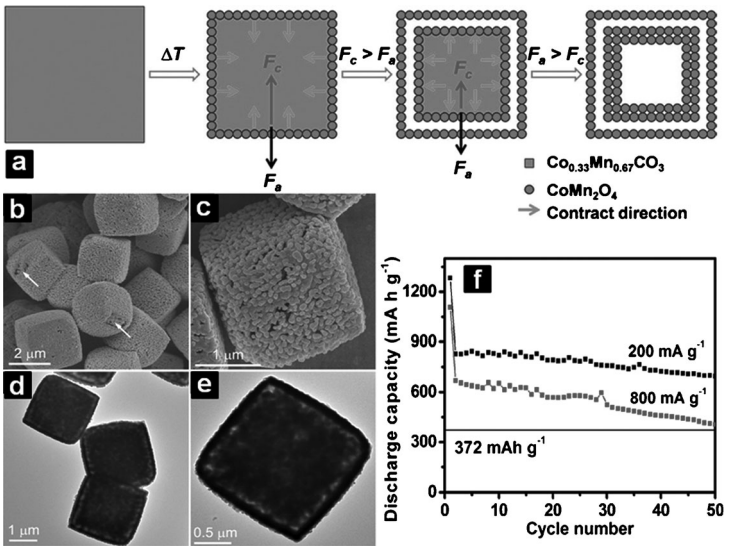

Figure 6. a) Illustration of the fabrication of double-shelled $CoMn_2O_4$ hollow microcubes. Typical b), c) FESEM and d), e) TEM images, and f) specific capacity as a function of cycle number for double-shelled hollow $CoMn_2O_4$ microcubes. Panels (a–f) are reproduced with permission:[9] Copyright 2012, Wiley.

to the large specific capacity; and 2) the hollow interior and the porosity in the shells can buffer the large volume change of anodes based on the conversion reaction during the repeated Li^+ insertion/extraction, thus alleviating the pulverization problem and enhancing the cycling performance.

One interesting member of these manganites is $ZnMn_2O_4$, which has been investigated as intriguing anode materials for LIBs owing to the low price, abundance, and environmental friendliness of both Zn and Mn species. This compound has a normal spinel structure with the bivalent Zn^{2+} ions occupying the tetrahedral sites and the trivalent Mn^{3+} ions occupying the octahedral sites in the cubic spinel structure. Interestingly, it can store Li^+ through not only the conversion reaction ($ZnMn_2O_4 + 8Li^+ + 8e^- \rightleftharpoons Zn + 2Mn + 4Li_2O$; $Zn + Li_2O \rightleftharpoons ZnO + 2Li^+ + 2e^-$; and $Mn + Li_2O \rightleftharpoons MnO + 2Li^+ + 2e^-$) but also the alloying reaction between Zn and Li ($Zn + Li^+ + e^- \rightleftharpoons LiZn$), leading to a high theoretical capacity of 784 mA h g^{-1}. $ZnMn_2O_4$ materials with various nanostructures (for example, NPs,[42,97] NWs),[34] and hierarchical micro-/nanostructures (such as nanoplate assemblies,[46] flower-like superstructure,[59] hollow microspheres,[95] and ball-in-ball hollow microspheres)[11] have been extensively investigated as anode materials for high-performance LIBs.

Recently, a novel template-free method was demonstrated to prepare unique ball-in-ball hollow $ZnMn_2O_4$ microspheres (Figure 7 a–d).[11] The ball-in-ball hollow microspheres typically consist of small NPs building blocks with an average size of about 30 nm, and exhibit a mesoporous feature with a narrow PSD centered at about 16 nm. When evaluated as an anode material for LIBs, the $ZnMn_2O_4$ ball-in-ball hollow microspheres show greatly enhanced electrochemical performance with high capacity, excellent cycling stability, and good rate capability. As seen in Figure 7 e, the capacity reaches a value as high as 750 mA h g^{-1} after 120 cycles at 400 mA g^{-1}, which is close to its theoretical capacity.

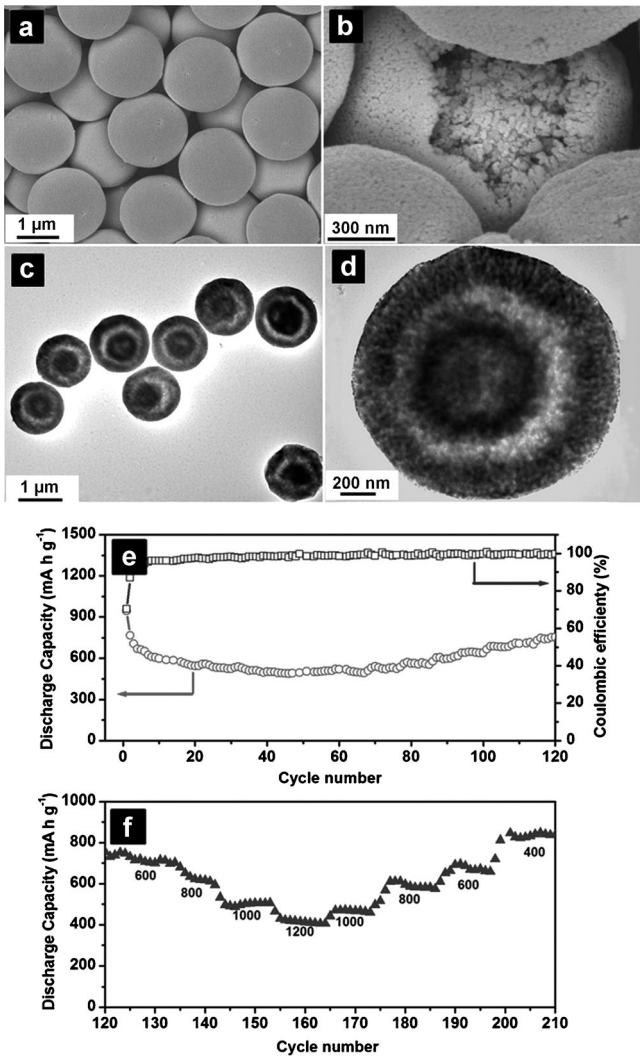

Figure 7. Typical a), b) FESEM and c), d) TEM images of $ZnMn_2O_4$ ball-in-ball hollow microspheres. e) Cycling performance at 400 mA g^{-1} and corresponding coulombic efficiency. f) Rate capability test at various current densities indicated in the unit of mA g^{-1} for the same cell after the cycling for 120 cycles at 400 mA g^{-1} as shown in (e). Panels (a–f) are reproduced with permission:[11] Copyright 2012, Wiley.

Then the same cell is further subjected to rate capability test at various current densities (Figure 7 f), with the average specific capacities of 683, 618, 480, and 396 mA h g^{-1} obtained at the current densities of 600, 800, 1000, 1200 mA g^{-1}, respectively. When the current density is reduced stepwise to 400 mA g^{-1} again, a specific capacity as high as 790 mA h g^{-1} is recovered. The exceptional electrochemical performance of the unique ball-in-ball hollow microspheres should be attributed to the unique microstructure. Specifically, the small average size of the primary NPs in the ball-in-ball hollow microspheres provides a short pathway for Li^+ diffusion, and the empty space serves as a reservoir for electrolyte, hence leading to good rate capability. Moreover, the unique ball-in-ball hollow architecture could significantly improve the structural integrity by partly mitigating the mechanical strain induced by volume change associated with the repeated Li^+ insertion/extraction processes during cycling,

which might contribute greatly to the excellent cycling stability. More significantly, with minor modifications, this strategy, as a simple and scalable synthesis approach, can be extended easily to fabricate other complex hollow structures of multi-component functional oxide materials.

The extended applications of Mn-based MTMOs in ECs have also been documented. The spinel $NiMn_2O_4$, in contrast to the Ni-Mn mixed oxides and mesoporous Mn_3O_4 materials, has several advantages, such as good conductivity, low cost, good structural stability, and relatively high SCs.[44,98] As an example, Liu et al.[44] developed an epoxide-driven sol–gel process coupled with calcination treatment to synthesize $NiMn_2O_4$ aerogel with mesopores of 8–10 nm in size, and a SSA of 201 $m^2 g^{-1}$. With these intriguing structural features, the as-prepared $NiMn_2O_4$ aerogel delivers a SC as high as 243 $F g^{-1}$ at 5 $mV s^{-1}$. More impressively, a SC of 169 $F g^{-1}$ is still obtained, and 96% of the initial SC value can be maintained after 5000 cycles at 20 $mV s^{-1}$ in 1 M Na_2SO_4 aqueous solution.

Similar to cobaltites, the appealing spinel manganites, as promising alternative electrocatalysts, have been studied as electrocatalysts for the ORR. Recently, Chen et al.[16] presented a facile and rapid room-temperature method for selective synthesis of the $CoMn_2O_4$ NPs with cubic or tetragonal structures, and studied their electrocatalytic ORR performance in alkaline media. The $CoMn_2O_4$ NPs manifest considerable catalytic activity towards the ORR as a result of their high SSA and abundant defects. Of particular note, the cubic spinel $CoMn_2O_4$ outperforms the tetragonal phase in intrinsic ORR electrocatalytic activity. The phase-dependent electrocatalytic ORR activities of the prepared $CoMn_2O_4$ are interpreted by both experimental and first-principles theoretical studies. Generally, the electrocatalytic ORR in alkaline system proceeds through multi-step reactions. HO_2^- intermediates are first formed from adsorbed O_2 on the active sites of the catalyst surface, followed by their further reduction or decomposition to OH^- ions. Thus, electrocatalytic activity of the ORR correlates with the number of available catalytic sites and the adsorption affinity for oxygen.

As shown in Figure 8 a–d, the cobalt defect sites can bind oxygen slightly more strongly than the manganese defect site, whereas on either the cobalt or manganese sites the cubic (113) surface generates much more stable molecular oxygen adducts than the tetragonal (121) surface, as revealed by the binding energies (E_b) of an oxygen molecule on Co/Mn defect sites. Also, the cubic phase shows an increase in the adsorbed oxygen-induced d-band, indicating a strengthened metal–O_2 bond in comparison with the tetragonal spinel phase, as observed in Figure 8 e, f. Moreover, the investigated surfaces of both phases contain the same number of catalytic sites per surface unit cell, whereas the area of the cubic (113) unit cell is smaller. Therefore, for a given surface area, the number of available active sites of the cubic (113) surface exceeds that on the tetragonal (121) surface. All of these are responsible for the enhanced ORR catalytic activity of cubic spinel $CoMn_2O_4$. The cubic spinel $CoMn_2O_4$ is further used in an air electrode to construct a coin-type Zn–air cell, which delivers a stable galvanostatic discharge curve and considerable specific energy density, showing its promising application in metal–air batteries.

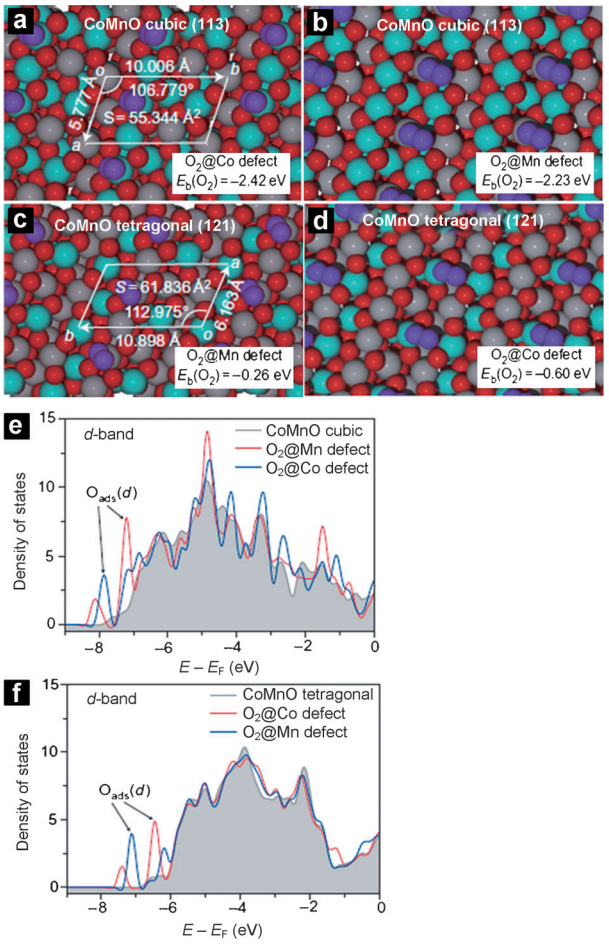

Figure 8. First-principles study of surface oxygen adsorption on different sites of cubic and tetragonal phases of $CoMn_2O_4$. a)–d) Geometries and binding energies of oxygen molecules (purple) on cobalt (cyan) or manganese (gray) defect sites. Red spheres represent lattice oxygen; S = area of the unit cell. e), f) Corresponding density of states of bare and O_2-adsorbed $CoMn_2O_4$. Panels (a–d) are reproduced with permission:[16] Copyright 2011, Nature Publishing Group.

As spinel $CoMn_2O_4$ is a semiconductor and good catalytic activity requires fast electron transport, the spinel $CoMn_2O_4$ NPs also need necessary attachment to a conducting surface, preferably a carbon surface. Among the myriad carbon materials, GNs with large SSA, high mechanical strength and electrical conductivity, as well as the intrinsic ORR activity owing to the abundant defects, have drawn much attention.[73] However, the published data indicates that the activity of GNs alone is insufficient.[77,99] Goodenough et al. developed a two-step synthesis route to directly grow spinel $CoMn_2O_4$ NPs on the surface of GNs, and used the nanocomposite material as ORR electrocatalysts for Li–O_2 batteries with both non-aqueous and aqueous electrolytes.[77] Electrochemical results based on rotating-disk-electrode tests indicate that such a nanostructured hybrid electrocatalyst has considerable catalytic ORR activity for lithium–air primary or rechargeable batteries of high energy density.

3.3. Ferrites

Recently, iron oxides with impressive electrochemical properties have received an upsurge of interest owing to the fascinating advantageous attributes, including low cost, environmental benignity, and high abundance. Nevertheless, when applied as an anode material, the higher oxidation potential, limited conductivity, and reaction kinetics restrict the battery output voltage and energy density.[100,101] Furthermore, poor capacity retention also remains a major drawback, owing to the serious electrode pulverization related to the huge volumetric expansion/contraction during the charge–discharge process. Thereby, the spinel MFe_2O_4 series (M = Co,[23,65,67,102–105] Ni,[37,66,102,106,107] Cu,[23,43,55,108] Mg,[60,109] Mn,[48,110] Ca,[111] and Zn[12,47,54,112,113]) have been extensively regarded as promising anodes for LIBs. It is highly anticipated that the existence of the other metal cation can effectively overcome the drawbacks of simple Fe-based oxides, and deliver larger specific capacity, better cycling stability, and rate performance by the careful selection of suitable combination of different metal species.

Similar to $ZnMn_2O_4$, $ZnFe_2O_4$ also stands out from the other ferrites as an attractive anode. Besides some common advantages such as low toxicity, easy synthesis, and low cost, $ZnFe_2O_4$ exhibits a relatively low working voltage of about 1.5 V, which is much lower than that of Co-based anodes (ca. 2.1 V),[78] Fe_2O_3 nanotubes arrays (ca. 1.74 V),[100] and Fe_2O_3 nanoflakes (ca. 2.1 V).[101] Therefore an enhanced output voltage of the full cell is anticipated when coupled with a conventional cathode material such as $LiCoO_2$.[54,112,113] Furthermore, it is also interesting to note that $ZnFe_2O_4$ gives a high theoretical specific capacity of 1072 $mA\,h\,g^{-1}$ owing to the simultaneous implementation of both conversion and alloying reactions to reversibly store lithium, which is similar to the case of $ZnMn_2O_4$ as mentioned earlier.[12] As the first report of nanocrystalline $ZnFe_2O_4$ and Ag-doped $ZnFe_2O_4$ thin films used as anodes for LIBs,[112] many endeavors have been devoted to further optimize the performance of $ZnFe_2O_4$ anode materials with different structures and morphologies by various synthesis strategies, including NPs prepared by a urea combustion method,[113] octahedra synthesized by a one-step hydrothermal route,[47] hollow microspheres synthesized by a hydrothermal reaction followed by annealing,[54] and so on.

Recently, Srinivasan et al.[12] developed a relatively cost-effective and simple electrospinning technique to synthesize nanowebs consisting of interwoven $ZnFe_2O_4$ NFs, and then used the obtained NFs as an environmentally friendly anode in LIBs. As shown in Figure 9a–d, the electrospun polycrystalline $ZnFe_2O_4$ NFs composed of 11 nm nanocrystal building blocks are self-assembled into intertwined porous nanowebs with a continuous framework. The electrospun nanowebs anode with $ZnFe_2O_4$ NFs exhibits excellent cyclability and retains a reversible capacity of 733 $mA\,h\,g^{-1}$ up to 30 cycles at 60 $mA\,g^{-1}$. Furthermore, the rate capability examined by galvanostatic cycling at various current densities for 55 cycles (Figure 9e) shows a high capacity of about 400 $mA\,h\,g^{-1}$ at 800 $mA\,g^{-1}$. The enhanced electrochemical performance of $ZnFe_2O_4$ NFs can be attributed to the continuous framework

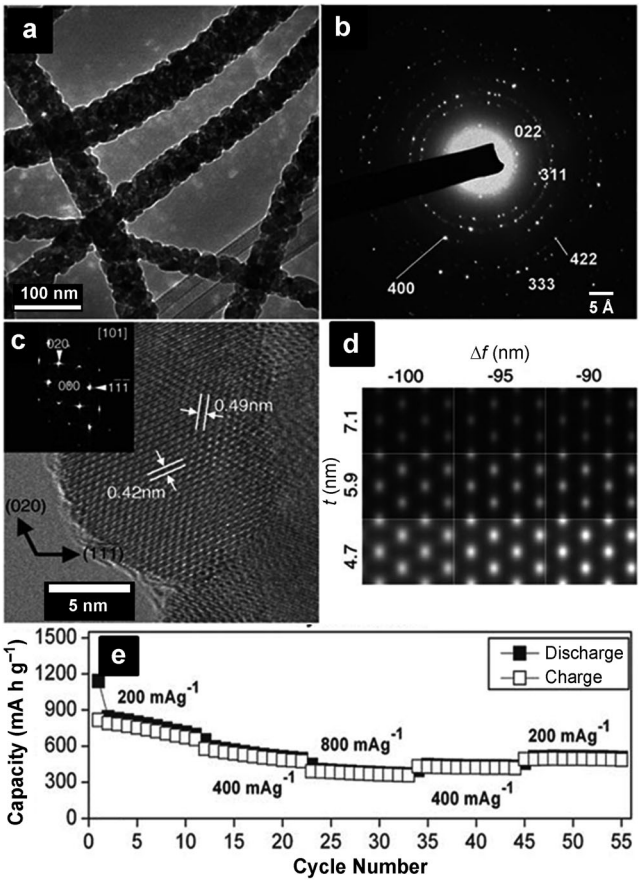

Figure 9. a) TEM micrograph of $ZnFe_2O_4$ NFs. b) SAED pattern. c) HRTEM image taken along the [101] zone axis; the inset is the corresponding fast Fourier transform pattern. d) Simulated HRTEM patterns showing that the thickness of this crystal is calculated to be about 5 nm. e) Capacity as a function of cycle number for the $ZnFe_2O_4$ NFs at various current densities. Panels (a–e) are reproduced with permission:[12] Copyright 2011, RSC.

with open pores for lithiation/delithiation in nanowebs. Moreover, the importance of providing electrical wiring in LIBs during prolonged cycling is especially emphasized.

Some other attractive ferrites, including $NiFe_2O_4$,[24,107,114] $CoFe_2O_4$,[21] and $MnFe_2O_4$,[115–117] are also investigated as pseudocapacitive materials for high-performance ECs. Among the three ferrites, $MnFe_2O_4$ exhibits unusually large pseudocapacitance arising from electron transfer of the Mn ions at the tetrahedral sites of the spinel structure, balanced by the intercalation of cations, such as Na^+ and K^+, from the aqueous solution, whereas the other ferrites do not.[115] Crystallographic and electrochemical data reveal that the appealing pseudocapacitive capacitance results from the crystalline rather than amorphous $MnFe_2O_4$ phase, and can give a gravimetric SC over 100 $F\,g^{-1}$, or a superficial areal SC of about 112 $\mu F\,cm^{-2}$. Of great interest, $MnFe_2O_4$ also exhibits typical capacitive characteristics with a SC of 126 $F\,g^{-1}$ in the organic electrolyte of $LiPF_6$ in a mixture of ethyl carbonate/ethylene methyl carbonate with a working voltage window up to 4.5 V vs. Li/Li^+.[116] An asymmetric acetylene black/$MnFe_2O_4$ cell configuration with such an organic electrolyte

has also been fabricated. The cell demonstrates superior stability under high-rate cycling in a working voltage window of 2.5 V, which is related to its small volume variation of $MnFe_2O_4$ in the charge–discharge process. The organic electrolyte system for peudocapacitive MTMOs is greatly beneficial for the significant enhancement of energy density of ECs, which is due to the simultaneous achievement of large working voltage window and high SC in organic electrolytes.

3.4. Stannates

Apart from the above-mentioned MTMOs that typically incorporate two types of transition-metal cations, mixed metal oxides based on tin (Sn) also receive much attention because of the exceptional lithium storage properties. Commonly, the lithium storage of simple tin-based metal oxides mainly relies on the reversible alloying–dealloying reaction between lithium and metallic Sn nanocrystals generated from the initial irreversible reduction of tin oxides. This class of materials generally delivers high capacity (for example, ca. 790 mA h g^{-1} for SnO_2) at a relatively low potential below 1.0 V (vs. Li/Li^+), and thus can be combined with some high-voltage cathodes to render LIBs with higher energy density. However, the severe pulverization caused by the drastic volume variation of more than 200% during repeated charge–discharge induces disintegration and loss of electrical contact, which eventually results in quick capacity fading.[118] One efficient way to alleviate the problem relies on the introduction of a foreign matrix to form composites with Sn-based materials and buffer the mechanical strain. Such matrixes could be other metal oxides or intermetallics (active or inactive towards Li), or carbonaceous materials. In this regard, Sn-based inverse spinel M_2SnO_4 (M = Mg, Mn, Co, and Zn),[119–122] and even non-spinel $MSnO_3$ (M = Ca, Co)[69,123,124] mixed metal oxides are anticipated to be appealing anodes for high-performance LIBs. Notably, the other metal species can function as both the buffer matrix and active component, which therefore raises the capacity without increasing the irreversible loss, and helps to cushion the expansion of Sn NCs upon lithiation.[121] Moreover, compared with simple tin oxides, the other metal oxide in the mixed oxides serves as a superior matrix for lithium oxide, which improves the overall performance of the Sn-based electrodes.[121] If Sn-based mixed metal oxides are made with desirable structure, morphology, and texture, exceptional electrochemical performance can be obtained. For example, a hollow structure has been widely adopted in many metal oxide electrode materials for its capability to achieve enhanced electrochemical performance by promoting the Li^+ diffusion and accommodating the lithium insertion strain.[69] The formation of a homogeneous amorphous structure also facilitates the lithium diffusion by improving the atomic/ionic mobility within the matrix.[69,125]

Motivated by the above rationale, the carbon-coated hollow nanostructure of amorphous $CoSnO_3$ has been recently developed[69] as a durable Sn-based anode material with satisfactory cycling stability and high reversibility. The $CoSnO_3$ nanoboxes with a homogeneous amorphous texture and high porosity are obtained by thermally induced dehydration of a $CoSn(OH)_6$ precursor,[69,126] and further coated with a continuous amorphous carbon overlayer with a uniform thickness of about 10 nm (Figure 10a–e). The high-quality $CoSnO_3$@C nanoboxes that were thus produced incorporate

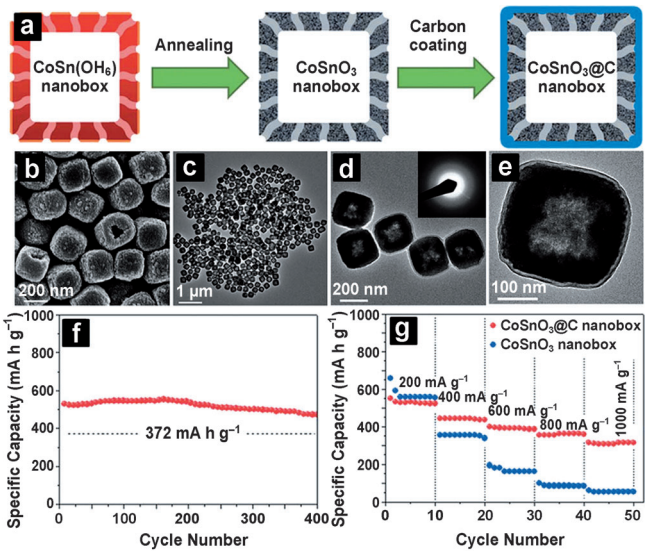

Figure 10. a) Illustration for the formation of amorphous $CoSnO_3$ nanoboxes with carbon nanocoating. b) FESEM and c), d) TEM images of $CoSnO_3$@C nanoboxes, of which the SEAD pattern is shown in the inset of (d). e) TEM image of a single $CoSnO_3$@C nanobox. f) Cycling stability of $CoSnO_3$@C nanoboxes at 200 mA g^{-1}, and g) rate capability of $CoSnO_3$ nanoboxes with and without carbon nanocoating. Panels (a–g) are reproduced with permission:[69] Copyright 2013, RSC.

several desirable design rationales, including hollow nanostructures, carbon nanopainting, a mixed conductive matrix, and crystalline texture engineering. In such a structure, the combination of hollow interior space and an elastic buffering carbon shell results in a highly flexible architecture to facilitate efficient lithium storage. In favor of the synergy and interplay of the matrix effect and intrinsic amorphous structural advantages, the $CoSnO_3$@C nanoboxes exhibit an exceptional cycle life of over 400 cycles (Figure 10f) and improved high-rate capability (450–310 mA h g^{-1} at high current densities of 400–1000 mA g^{-1}; Figure 10g) when evaluated as an anode material for LIBs.

4. Outlook and Challenges

In this Review, we have summarized the recent progress in the field of rational design and synthesis of intriguing MTMOs with various architectures and compositions, and highlighted their promising applications in energy storage/conversion technologies, including LIBs, ECs, MOBs, and FCs. The complex chemical compositions and the synergic effects of multiple metal species in these MTMOs give rise to their remarkable electrochemical performance. As discussed above, several elegant strategies, such as manipulation of the micro-/nanostructures and compositions, have been exten-

sively developed, with the ultimate aim to boost the electrochemical performance and promote the practical use of MTMOs in energy storage/conversion devices. Nevertheless, each design strategy applied alone commonly results in limited enhancement in electrochemical performance of MTMO-based electrodes. Therefore, it is more compelling to integrate multiple interesting design strategies, thus maximizing their electrochemical advantages to meet the present energy demands.

Encouragingly, spinel MTMOs have already been demonstrated to show promising performance as electrode materials for LIBs and ECs, and advanced ORR electrocatalysts for MOBs and FCs. However, the majority of the reports regarding the applications of MTMOs in these energy systems with promising enhancement are mainly based on individual experimental observations. A comprehensive and in-depth insight into the relationship between the structure/composition and the property/performance of these MTMOs has not yet been systematically achieved. Therefore, there is an urgent need to develop efficient and reliable methods and criteria to evaluate the MTMO-based energy-related devices. The establishment of mathematical modeling and theoretical simulation is also highly anticipated to direct the purposeful design and facile, large-scale, and low-cost fabrication of MTMOs with superior electrochemical performance.

Understanding the failure mechanisms upon cycling in these MTMO-based electrodes for LIBs and ECs is crucial to guide the design of advanced materials. This requires not only understanding the structure evolution and composition regulation, but also taking electrolyte compatibility issues into consideration. It has been demonstrated that modification of the electrolytes, such as some reversible redox couples as additives in aqueous electrolytes,[127] could significantly improve the overall electrochemical performance of pseudocapacitive materials. Therefore, we also expect that the proper design of electrolytes for both rechargeable batteries and ECs could further optimize the electrochemical behavior of the MTMOs. Furthermore, the evaluation of pseudocapacitive performance of MTMOs as the electroactive materials for ECs is mainly performed in aqueous electrolytes, which inevitably limits the energy density due to the narrow stable potential window of aqueous electrolytes. To maximize the operating voltage output, some non-aqueous organic electrolytes have been studied as desirable candidates,[116,128] which typically provide a two or three times wider working voltage window than the aqueous ones. Therefore, the exploration of MTMO-based ECs with organic electrolytes is of high importance to obtain higher energy/power density that will greatly pave the way for the practical use of ECs. Apart from evaluation based on electrochemical performance, other issues regarding safety, environmental compatibility, cost, and ease of manipulation and fabrication should also be taken into serious consideration when developing industrially applicable MTMOs for LIBs and ECs. It should be stressed that the synthesis of these MTMO materials should be easily scalable for commercial applications.

The electrochemical reduction of oxygen on MTMO catalysts is a complex process, which could involve different mechanisms determined by the nature of MTMOs, including their physicochemical and adsorption properties. To date, there have not been many such studies that are particularly focused on the kinetics and mechanisms of electrochemical oxygen reduction on MTMOs, the influence of catalyst characteristics and adsorbed oxygen on the reaction rate, and the intrinsic interactions between MTMO catalysts and carbonaceous matrixes. One difficulty of investigating the electrochemical processes on MTMOs is associated with their semiconducting properties, which can lead to different behaviors of the reactions on MTMOs catalysts, as compared to metal-based catalysts. Future development might lead to highly efficient and economical MTMO catalysts after some optimization among electrocatalytic activity, thermodynamic stability, corrosion resistance, fabrication cost, and long-term stability, which would provide a major boost for the relevant energy technologies towards their aspired commercialization.

Despite the challenges ahead, there is hope that MTMOs will be the materials platform in the near future for breaking many of the current bottlenecks of clean and renewable energy storage/conversion technologies. To achieve this goal, significant advances need to be made on the electrochemical performance and in-depth understanding of mechanisms of the MTMOs in energy storage/conversion applications. With sustained and dedicated research efforts, these intriguing MTMO nanomaterials would offer a new avenue to make the attractive energy technologies commercially viable.

Y.X. acknowledges the financial support from National Natural Science Foundation of China (11079004, 90922016).

Received: May 9, 2013
Published online: January 2, 2014

[1] A. L. M. Reddy, S. R. Gowda, M. M. Shaijumon, P. M. Ajayan, *Adv. Mater.* **2012**, *24*, 5045 – 5064.
[2] Z. Yang, J. Zhang, M. C. W. Kintner-Meyer, X. Lu, D. Choi, J. P. Lemmon, J. Liu, *Chem. Rev.* **2011**, *111*, 3577 – 3613.
[3] A. S. Aricò, P. Bruce, B. Scrosati, J.-M. Tarascon, W. van Schalkwijk, *Nat. Mater.* **2005**, *4*, 366 – 377.
[4] P. Simon, Y. Gogotsi, *Nat. Mater.* **2008**, *7*, 845 – 854.
[5] J. Jiang, Y. Li, J. Liu, X. Huang, C. Yuan, X. W. Lou, *Adv. Mater.* **2012**, *24*, 5166 – 5180.
[6] C. Liu, F. Li, L.-P. Ma, H.-M. Cheng, *Adv. Mater.* **2010**, *22*, E28 – E62.
[7] A. Manthiram, A. Vadivel Murugan, A. Sarkar, T. Muraliganth, *Energy Environ. Sci.* **2008**, *1*, 621 – 638.
[8] J. B. Goodenough, K.-S. Park, *J. Am. Chem. Soc.* **2013**, *135*, 1167 – 1176.
[9] L. Zhou, D. Zhao, X. W. Lou, *Adv. Mater.* **2012**, *24*, 745 – 748.
[10] T.-Y. Wei, C.-H. Chen, H.-C. Chien, S.-Y. Lu, C.-C. Hu, *Adv. Mater.* **2010**, *22*, 347 – 351.
[11] G. Zhang, L. Yu, H. B. Wu, H. E. Hoster, X. W. Lou, *Adv. Mater.* **2012**, *24*, 4609 – 4613.
[12] P. F. Teh, Y. Sharma, S. S. Pramana, M. Srinivasan, *J. Mater. Chem.* **2011**, *21*, 14999 – 15008.
[13] Z. Wang, L. Zhou, X. W. Lou, *Adv. Mater.* **2012**, *24*, 1903 – 1911.
[14] M. Hamdani, R. N. Singh, P. Chartier, *Int. J. Electrochem. Sci.* **2010**, *5*, 556 – 577.
[15] Y. Liang, H. Wang, J. Zhou, Y. Li, J. Wang, T. Regier, H. Dai, *J. Am. Chem. Soc.* **2012**, *134*, 3517 – 3523.
[16] F. Cheng, J. Shen, B. Peng, Y. Pan, Z. Tao, J. Chen, *Nat. Chem.* **2011**, *3*, 79 – 84.

[17] L. Hu, L. Wu, M. Liao, X. Hu, X. Fang, *Adv. Funct. Mater.* **2012**, *22*, 998 – 1004.
[18] S. Trasatti, *Electrodes of conductive metallic oxides Part A*, Elsevier Scientific Pub. Co., **1980**, p. 227.
[19] Q. Lu, J. G. Chen, J. Q. Xiao, *Angew. Chem.* **2013**, *125*, 1932 – 1940; *Angew. Chem. Int. Ed.* **2013**, *52*, 1882 – 1889.
[20] G. Wang, L. Zhang, J. Zhang, *Chem. Soc. Rev.* **2012**, *41*, 797 – 828.
[21] D. H. Deng, H. Pang, J. M. Du, J. W. Deng, S. J. Li, J. Chen, J. S. Zhang, *Cryst. Res. Technol.* **2012**, *47*, 1032 – 1038.
[22] F. M. Courtel, H. Duncan, Y. Abu-Lebdeh, I. J. Davidson, *J. Mater. Chem.* **2011**, *21*, 10206 – 10218.
[23] Y.-N. NuLi, Q.-Z. Qin, *J. Power Sources* **2005**, *142*, 292 – 297.
[24] S. Anwar, K. S. Muthu, V. Ganesh, N. Lakshminarasimhan, *J. Electrochem. Soc.* **2011**, *158*, A976 – A981.
[25] S. Sun, Z. Wen, J. Jin, Y. Cui, Y. Lu, *Microporous Mesoporous Mater.* **2013**, *169*, 242 – 247.
[26] N. Bahlawane, P. H. T. Ngamou, V. Vannier, T. Kottke, J. Heberle, K. Kohse-Hoeinghaus, *Phys. Chem. Chem. Phys.* **2009**, *11*, 9224 – 9232.
[27] Y. Sharma, N. Sharma, G. V. S. Rao, B. V. R. Chowdari, *Solid State Ionics* **2008**, *179*, 587 – 597.
[28] B. Ellis, P. Subramanya Herle, Y. H. Rho, L. F. Nazar, R. Dunlap, L. K. Perry, D. H. Ryan, *Faraday Discuss.* **2007**, *134*, 119 – 141.
[29] D. Pasero, N. Reeves, A. R. West, *J. Power Sources* **2005**, *141*, 156 – 158.
[30] W. Luo, X. Hu, Y. Sun, Y. Huang, *J. Mater. Chem.* **2012**, *22*, 8916 – 8921.
[31] G. Zhang, B. Y. Xia, C. Xiao, L. Yu, X. Wang, Y. Xie, X. W. Lou, *Angew. Chem.* **2013**, *125*, 8805 – 8809; *Angew. Chem. Int. Ed.* **2013**, *52*, 8643 – 8647.
[32] N. Du, Y. Xu, H. Zhang, J. Yu, C. Zhai, D. Yang, *Inorg. Chem.* **2011**, *50*, 3320 – 3324.
[33] H. Jiang, J. Ma, C. Li, *Chem. Commun.* **2012**, *48*, 4465 – 4467.
[34] S.-W. Kim, H.-W. Lee, P. Muralidharan, D.-H. Seo, W.-S. Yoon, D. K. Kim, K. Kang, *Nano Res.* **2011**, *4*, 505 – 510.
[35] H. Wang, Q. Gao, L. Jiang, *Small* **2011**, *7*, 2454 – 2459.
[36] C. Yuan, J. Li, L. Hou, L. Yang, L. Shen, X. Zhang, *J. Mater. Chem.* **2012**, *22*, 16084 – 16090.
[37] D. Zhang, Z. Tong, G. Xu, S. Li, J. Ma, *Solid State Sci.* **2009**, *11*, 113 – 117.
[38] G. Q. Zhang, H. B. Wu, H. E. Hoster, M. B. Chan-Park, X. W. Lou, *Energy Environ. Sci.* **2012**, *5*, 9453 – 9456.
[39] C. Yuan, J. Li, L. Hou, X. Zhang, L. Shen, X. W. Lou, *Adv. Funct. Mater.* **2012**, *22*, 4592 – 4597.
[40] G. Q. Zhang, X. W. Lou, *Adv. Mater.* **2013**, *25*, 976 – 979.
[41] Y. Q. Wu, X. Y. Chen, P. T. Ji, Q. Q. Zhou, *Electrochim. Acta* **2011**, *56*, 7517 – 7522.
[42] Y. Yang, Y. Zhao, L. Xiao, L. Zhang, *Electrochem. Commun.* **2008**, *10*, 1117 – 1120.
[43] H. Zhao, H. Jia, S. Wang, D. Xue, Z. Zheng, *J. Exp. Nanosci.* **2011**, *6*, 75 – 83.
[44] M. Zhang, S. Guo, L. Zheng, G. Zhang, Z. Hao, L. Kang, Z.-H. Liu, *Electrochim. Acta* **2013**, *87*, 546 – 553.
[45] H.-C. Chien, W.-Y. Cheng, Y.-H. Wang, S.-Y. Lu, *Adv. Funct. Mater.* **2012**, *22*, 5038 – 5043.
[46] J. Zhao, F. Wang, P. Su, M. Li, J. Chen, Q. Yang, C. Li, *J. Mater. Chem.* **2012**, *22*, 13328 – 13333.
[47] Z. Xing, Z. Ju, J. Yang, H. Xu, Y. Qian, *Nano Res.* **2012**, *5*, 477 – 485.
[48] D. Zhang, X. Zhang, X. Ni, J. Song, H. Zheng, *Chem. Phys. Lett.* **2006**, *426*, 120 – 123.
[49] X. Lai, J. E. Halpert, D. Wang, *Energy Environ. Sci.* **2012**, *5*, 5604 – 5618.
[50] X. W. Lou, L. A. Archer, Z. Yang, *Adv. Mater.* **2008**, *20*, 3987 – 4019.
[51] Q. Wang, B. Liu, X. Wang, S. Ran, L. Wang, D. Chen, G. Shen, *J. Mater. Chem.* **2012**, *22*, 21647 – 21653.
[52] T. Wu, J. Y. Li, L. R. Hou, C. Z. Yuan, L. Yang, X. G. Zhang, *Electrochim. Acta* **2012**, *81*, 172 – 178.
[53] J. Xiao, S. Yang, *RSC Adv.* **2011**, *1*, 588 – 595.
[54] X. Guo, X. Lu, X. Fang, Y. Mao, Z. Wang, L. Chen, X. Xu, H. Yang, Y. Liu, *Electrochem. Commun.* **2010**, *12*, 847 – 850.
[55] L. Jin, Y. Qiu, H. Deng, W. Li, H. Li, S. Yang, *Electrochim. Acta* **2011**, *56*, 9127 – 9132.
[56] J. Li, S. Xiong, X. Li, Y. Qian, *Nanoscale* **2013**, *5*, 2045 – 2054.
[57] J. F. Li, S. L. Xiong, Y. R. Liu, Z. C. Ju, Y. T. Qian, *ACS Appl. Mater. Interfaces* **2013**, *5*, 981 – 988.
[58] J. Li, S. Xiong, X. Li, Y. Qian, *J. Mater. Chem.* **2012**, *22*, 23254 – 23259.
[59] L. Xiao, Y. Yang, J. Yin, Q. Li, L. Zhang, *J. Power Sources* **2009**, *194*, 1089 – 1093.
[60] C. Gong, Y. J. Bai, Y. X. Qi, N. Lun, J. Feng, *Electrochim. Acta* **2013**, *90*, 119 – 127.
[61] Y. NuLi, P. Zhang, Z. Guo, H. Liu, J. Yang, *Electrochem. Solid-State Lett.* **2008**, *11*, A64 – A67.
[62] Q. Che, F. Zhang, X.-G. Zhang, X.-J. Lu, B. Ding, J.-J. Zhu, *Acta Phys.-Chim. Sin.* **2012**, *28*, 837 – 842.
[63] R. Ryoo, S. H. Joo, M. Kruk, M. Jaroniec, *Adv. Mater.* **2001**, *13*, 677 – 681.
[64] X. Wang, X. Han, M. Lim, N. Singh, C. L. Gan, M. Jan, P. S. Lee, *J. Phys. Chem. C* **2012**, *116*, 12448 – 12454.
[65] Y. Wang, J. Park, B. Sun, H. Ahn, G. Wang, *Chem. Asian J.* **2012**, *7*, 1940 – 1946.
[66] Y. S. Fu, Y. H. Wan, H. Xia, X. Wang, *J. Power Sources* **2012**, *213*, 338 – 342.
[67] S. Liu, J. Xie, C. Fang, G. Cao, T. Zhu, X. Zhao, *J. Mater. Chem.* **2012**, *22*, 19738 – 19743.
[68] Q. J. Xiang, J. G. Yu, M. Jaroniec, *Chem. Soc. Rev.* **2012**, *41*, 782 – 796.
[69] Z. Y. Wang, Z. C. Wang, W. T. Liu, W. Xiao, X. W. Lou, *Energy Environ. Sci.* **2013**, *6*, 87 – 91.
[70] B. Liu, J. Zhang, X. Wang, G. Chen, D. Chen, C. Zhou, G. Shen, *Nano Lett.* **2012**, *12*, 3005 – 3011.
[71] J. Liu, C. Liu, Y. Wan, W. Liu, Z. Ma, S. Ji, J. Wang, Y. Zhou, P. Hodgson, Y. Li, *CrystEngComm* **2013**, *15*, 1578 – 1585.
[72] L. Yu, G. Zhang, C. Yuan, X. W. Lou, *Chem. Commun.* **2013**, *49*, 137 – 139.
[73] E. Yoo, H. Zhou, *Acs Nano* **2011**, *5*, 3020 – 3026.
[74] V. S. Bagotzky, N. A. Shumilova, E. I. Khrushcheva, *Electrochim. Acta* **1976**, *21*, 919 – 924.
[75] P. A. Christensen, A. Hamnett, D. Linares-Moya, *Phys. Chem. Chem. Phys.* **2011**, *13*, 5206 – 5214.
[76] H. Wang, Y. Yang, Y. Liang, G. Zheng, Y. Li, Y. Cui, H. Dai, *Energy Environ. Sci.* **2012**, *5*, 7931 – 7935.
[77] L. Wang, X. Zhao, Y. Lu, M. Xu, D. Zhang, R. S. Ruoff, K. J. Stevenson, J. B. Goodenough, *J. Electrochem. Soc.* **2011**, *158*, A1379 – A1382.
[78] X. W. Lou, D. Deng, J. Y. Lee, J. Feng, L. A. Archer, *Adv. Mater.* **2008**, *20*, 258 – 262.
[79] B. Das, M. V. Reddy, G. V. S. Rao, B. V. R. Chowdari, *J. Mater. Chem.* **2012**, *22*, 17505 – 17510.
[80] R. Alcántara, M. Jaraba, P. Lavela, J. L. Tirado, *Chem. Mater.* **2002**, *14*, 2847 – 2848.
[81] P. Lavela, J. L. Tirado, C. Vidal-Abarca, *Electrochim. Acta* **2007**, *52*, 7986 – 7995.
[82] Y. Sharma, N. Sharma, G. V. S. Rao, B. V. R. Chowdari, *J. Power Sources* **2007**, *173*, 495 – 501.
[83] C. C. Ai, M. C. Yin, C. W. Wang, J. T. Sun, *J. Mater. Sci.* **2004**, *39*, 1077 – 1079.
[84] Y. Sharma, N. Sharma, G. V. Subba Rao, B. V. R. Chowdari, *Adv. Funct. Mater.* **2007**, *17*, 2855 – 2861.
[85] K. H. Chang, C. C. Hu, *Appl. Phys. Lett.* **2006**, *88*, 193102.

[86] D. N. Futaba, K. Hata, T. Yamada, T. Hiraoka, Y. Hayamizu, Y. Kakudate, O. Tanaike, H. Hatori, M. Yumura, S. Iijima, *Nat. Mater.* **2006**, *5*, 987 – 994.
[87] C. Wang, X. Zhang, D. Zhang, C. Yao, Y. Ma, *Electrochim. Acta* **2012**, *63*, 220 – 227.
[88] Q. Lu, Y. Chen, W. Li, J. G. Chen, J. Q. Xiao, F. Jiao, *J. Mater. Chem. A* **2013**, *1*, 2331 – 2336.
[89] H.-W. Wang, Z.-A. Hu, Y.-Q. Chang, Y.-L. Chen, H.-Y. Wu, Z.-Y. Zhang, Y.-Y. Yang, *J. Mater. Chem.* **2011**, *21*, 10504 – 10511.
[90] G. Zhang, X. W. Lou, *Sci. Rep.* **2013**, *3*, 1470.
[91] R. R. Salunkhe, K. Jang, H. Yu, S. Yu, T. Ganesh, S.-H. Han, H. Ahn, *J. Alloys Compd.* **2011**, *509*, 6677 – 6682.
[92] Q. Wang, X. Wang, B. Liu, G. Yu, X. Hou, D. Chen, G. Shen, *J. Mater. Chem. A* **2013**, *1*, 2468 – 2473.
[93] M. De Koninck, B. Marsan, *Electrochim. Acta* **2008**, *53*, 7012 – 7021.
[94] F. Bidault, D. J. L. Brett, P. H. Middleton, N. P. Brandon, *J. Power Sources* **2009**, *187*, 39 – 48.
[95] L. Zhou, H. B. Wu, T. Zhu, X. W. Lou, *J. Mater. Chem.* **2012**, *22*, 827 – 829.
[96] F. M. Courtel, Y. Abu-Lebdeh, I. J. Davidson, *Electrochim. Acta* **2012**, *71*, 123 – 127.
[97] Y. Deng, S. Tang, Q. Zhang, Z. Shi, L. Zhang, S. Zhan, G. Chen, *J. Mater. Chem.* **2011**, *21*, 11987 – 11995.
[98] J. A. Schmidt, A. E. Sagua, J. C. Bazán, M. R. Prat, M. E. Braganza, E. Morán, *Mater. Res. Bull.* **2005**, *40*, 635 – 642.
[99] L. Qu, Y. Liu, J.-B. Baek, L. Dai, *Acs Nano* **2010**, *4*, 1321 – 1326.
[100] J. Liu, Y. Li, H. Fan, Z. Zhu, J. Jiang, R. Ding, Y. Hu, X. Huang, *Chem. Mater.* **2010**, *22*, 212 – 217.
[101] M. V. Reddy, T. Yu, C.-H. Sow, Z. X. Shen, C. T. Lim, G. V. S. Rao, B. V. R. Chowdari, *Adv. Funct. Mater.* **2007**, *17*, 2792 – 2799.
[102] P. Lavela, J. L. Tirado, *J. Power Sources* **2007**, *172*, 379 – 387.
[103] M. Li, Y.-X. Yin, C. Li, F. Zhang, L.-J. Wan, S. Xu, D. G. Evans, *Chem. Commun.* **2012**, *48*, 410 – 412.
[104] Z. H. Li, T. P. Zhao, X. Y. Zhan, D. S. Gao, Q. Z. Xiao, G. T. Lei, *Electrochim. Acta* **2010**, *55*, 4594 – 4598.
[105] Y. Wang, D. W. Su, A. Ung, J. H. Ahn, G. X. Wang, *Nanotechnology* **2012**, *23*, 055402.
[106] R. Alcántara, M. Jaraba, P. Lavela, J. L. Tirado, J. C. Jumas, J. Olivier-Fourcade, *Electrochem. Commun.* **2003**, *5*, 16 – 21.
[107] B. Senthilkumar, R. K. Selvan, P. Vinothbabu, I. Perelshtein, A. Gedanken, *Mater. Chem. Phys.* **2011**, *130*, 285 – 292.
[108] M. Bomio, P. Lavela, J. L. Tirado, *J. Solid State Electrochem.* **2008**, *12*, 729 – 737.
[109] N. Sivakumar, S. R. P. Gnanakan, K. Karthikeyan, S. Amaresh, W. S. Yoon, G. J. Park, Y. S. Lee, *J. Alloys Compd.* **2011**, *509*, 7038 – 7041.
[110] Z. L. Zhang, Y. H. Wang, Q. Q. Tan, Z. Y. Zhong, F. B. Su, *J. Colloid Interface Sci.* **2013**, *398*, 185 – 192.
[111] N. Sharma, K. M. Shaju, G. V. S. Rao, B. V. R. Chowdari, *J. Power Sources* **2003**, *124*, 204 – 212.
[112] Y. N. NuLi, Y. Q. Chu, Q. Z. Qin, *J. Electrochem. Soc.* **2004**, *151*, A1077 – A1083.
[113] Y. Sharma, N. Sharma, G. V. S. Rao, B. V. R. Chowdari, *Electrochim. Acta* **2008**, *53*, 2380 – 2385.
[114] P. Sen, A. De, *Electrochim. Acta* **2010**, *55*, 4677 – 4684.
[115] S.-L. Kuo, N.-L. Wu, *Electrochem. Solid-State Lett.* **2005**, *8*, A495 – A499.
[116] S.-L. Kuo, N.-L. Wu, *Electrochem. Solid-State Lett.* **2007**, *10*, A171 – A175.
[117] Y.-P. Lin, N.-L. Wu, *J. Power Sources* **2011**, *196*, 851 – 854.
[118] J. S. Chen, X. W. Lou, *Small* **2013**, *9*, 1877 – 1893.
[119] F. Belliard, P. A. Connor, J. T. S. Irvine, *Solid State Ionics* **2000**, *135*, 163 – 167.
[120] P. A. Connor, J. T. S. Irvine, *J. Power Sources* **2001**, *97 – 98*, 223 – 225.
[121] P. A. Connor, J. T. S. Irvine, *Electrochim. Acta* **2002**, *47*, 2885 – 2892.
[122] A. Rong, X. P. Gao, G. R. Li, T. Y. Yan, H. Y. Zhu, J. Q. Qu, D. Y. Song, *J. Phys. Chem. B* **2006**, *110*, 14754 – 14760.
[123] F. Huang, Z. Y. Yuan, H. Zhan, Y. H. Zhou, J. T. Sun, *Mater. Lett.* **2003**, *57*, 3341 – 3345.
[124] N. Sharma, K. M. Shaju, G. V. Subba Rao, B. V. R. Chowdari, *Electrochem. Commun.* **2002**, *4*, 947 – 952.
[125] H. Li, P. Balaya, J. Maier, *J. Electrochem. Soc.* **2004**, *151*, A1878 – A1885.
[126] Z. Y. Wang, Z. C. Wang, H. B. Wu, X. W. Lou, *Sci. Rep.* **2013**, *3*, 1391.
[127] L.-H. Su, X.-G. Zhang, C.-H. Mi, B. Gao, Y. Liu, *Phys. Chem. Chem. Phys.* **2009**, *11*, 2195 – 2202.
[128] Y. Wang, Z. Hong, M. Wei, Y. Xia, *Adv. Funct. Mater.* **2012**, *22*, 5185 – 5193.